Atmospheric and upper ocean environments of Southern Ocean polar mesocyclones in the transition season months and associations with teleconnections

Chantal Claud, Andrew M. Carleton, Bertrand Duchiron, Pascal Terray

Atmospheric and upper ocean environments of Southern Ocean polar mesocyclones in the transition season months and associations with teleconnections

Chantal Claud,[1] Andrew M. Carleton,[2] Bertrand Duchiron,[1] and Pascal Terray[3]

Received 2 March 2009; revised 24 July 2009; accepted 31 August 2009; published 4 December 2009.

[1] Over middle and higher latitudes of the Southern Hemisphere, intense mesoscale cyclonic vortices that develop in cold-air outbreaks (cold-air mesocyclones) occur frequently during transition season months. In this study, previously published mesocyclone inventories for March–April and October–November are compared to atmospheric and upper ocean variables pertinent to mesocyclogenesis, as provided by reanalyses. This procedure allows the determination of the large-scale environments favorable for mesocyclone occurrence: low midtropospheric temperatures, greater sea ice extent, and large positive differences in the sea surface temperature minus low-altitude air temperature, the latter coinciding with enhanced low-level winds having a southerly component. We then evaluate the associations between polar mesocyclone formation and dominant patterns of low-frequency variability in the atmospheric circulation: the El Niño–Southern Oscillation (ENSO), the Southern Annular Mode (SAM), and the Trans-Polar Index (TPI). Our results suggest that in spring, the intrahemispheric variability in mesocyclogenesis is dominated by ENSO. In autumn, the influences of ENSO, SAM, and TPI on mesocyclone activity are about equal, although the response differs regionally. Moreover, teleconnections' effects on mesocyclone activity are somewhat reduced compared to that in spring. In both seasons, the phase of the semiannual oscillation modulates the associations with mesocyclones by influencing the latitude of the circumpolar trough and the amount of cyclonic activity over the Southern Ocean. These associations likely result from the displacement of the storm track between opposite phases of a given teleconnection and its position relative to the sea ice edge.

Citation: Claud, C., A. M. Carleton, B. Duchiron, and P. Terray (2009), Atmospheric and upper ocean environments of Southern Ocean polar mesocyclones in the transition season months and associations with teleconnections, *J. Geophys. Res.*, *114*, D23104, doi:10.1029/2009JD011995.

1. Introduction

[2] Over middle and higher latitudes of the Southern Hemisphere (SH) (Figure 1), intense mesoscale cyclonic vortices that develop in cold-air outbreaks, or cold-air mesocyclones [*Heinemann and Claud*, 1997], occur not only in the cold season but also during transition season months [e.g., *Carleton and Song*, 1997]. Previous studies even suggest a maximum frequency of systems in the months of March and October [e.g., *Turner and Row*, 1989; *Bromwich*, 1991; *Fitch and Carleton*, 1992; *Carleton and Song*, 1997; *Carrasco and Bromwich*, 1996; *Carrasco et al.*, 1997a, 1997b, 2003]. This situation contrasts with the Northern Hemisphere (NH), where mesocyclone maximum frequencies occur in winter [e.g., *Wilhelmsen*, 1985; *Harold et al.*, 1999; *Rasmussen and Turner*, 2003; *Blechschmidt*, 2008; *Bracegirdle and Gray*, 2008; *Zahn and von Storch*, 2008]. A likely explanation for the interhemispheric differences in mesocyclone seasonal activity is that Antarctica is a source of cold air throughout the year, and latitudinal temperature gradients are intensified over the sub-Antarctic in the equinoctial and immediately adjacent months accompanying the semiannual oscillation (SAO) of pressure/height and zonal winds [e.g., *van Loon*, 1967; *van Loon and Rogers*, 1984].

[3] Case studies of cold-air mesocyclones in the SH can be divided into two broad satellite-observed signature types, namely, comma-cloud and spiraliform vortices [e.g., *Forbes and Lottes*, 1985; *Carleton and Carpenter*, 1989; *Heinemann*, 1990; *Turner et al.*, 1993a; *Carleton*, 1995; *McMurdie et al.*, 1997]. The comma-cloud vortex type, with a length scale of 500–1000 km, typically represents deep baroclinicity and occurs in cold advection within the larger circulation of frontal cyclones [e.g., *Mansfield*, 1974; *Reed*, 1979; *Carleton*, 1987; *Businger and Reed*, 1989]. These systems are associated with Positive Vorticity Advection (PVA) at midtropospheric levels. The spiraliform

[1]Laboratoire de Météorologie Dynamique, IPSL, École Polytechnique, CNRS, Palaiseau, France.
[2]Department of Geography, and Earth and Environmental Systems Institute, Penn State University, University Park, Pennsylvania, USA.
[3]LOCEAN, IPSL, IRD, MNHN, Université Pierre et Marie Curie, CNRS, Paris, France.

0148-0227/09/2009JD011995

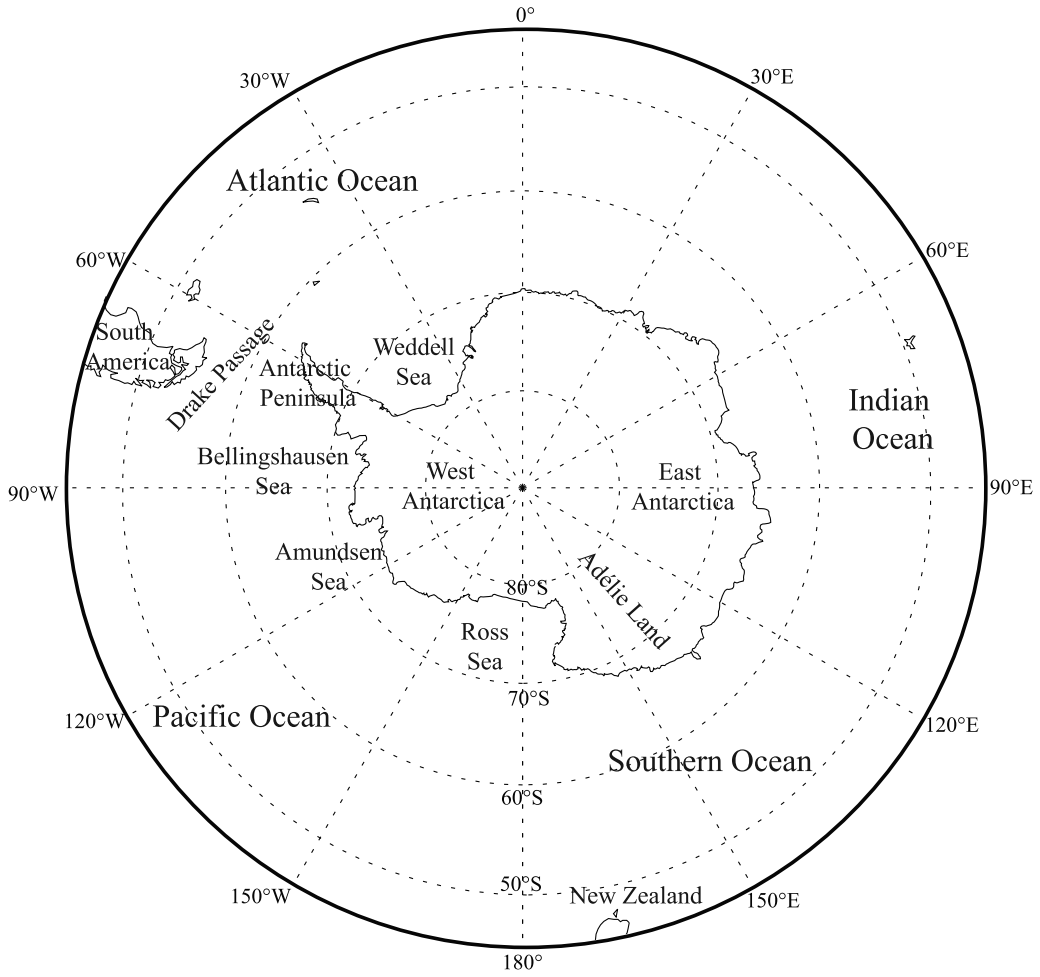

Figure 1. Map of Antarctica, indicating geographic features mentioned in the text.

vortex type, generally of smaller size, tends to occur at higher latitudes deep within cold air (i.e., more barotropic conditions [*Rasmussen*, 1979, 1981; *Rasmussen et al.*, 1992; *Turner et al.*, 1993a]). Moreover, most cold-air mesocyclones develop over the open sea where their intensity is enhanced by vertical fluxes of heat and moisture. This suggests that a wide variety of mechanisms can be important for the development and maintenance of cold-air mesocyclones. Indeed, a long-standing controversy existed on whether baroclinic instability [e.g., *Harrold and Browning*, 1969; *Mansfield*, 1974; *Duncan*, 1977; *Nordeng and Rasmussen*, 1992], conditional instability of the second kind (CISK), or wind-induced surface heat exchange (WISHE) [e.g., *Emanuel*, 1986; *Emanuel and Rotunno*, 1989; *Rasmussen*, 1989], would better explain such developments. A consensus was finally reached in 1994: mesocyclones appear in many forms, leading to the concept of a "spectrum" [*Turner et al.*, 1993a] extending from purely baroclinic to purely convective systems, and including hybrid systems.

[4] Because mesocyclones often are associated with significant weather (strong winds; heavy precipitation as rain, hail and/or snow; rough seas), and can develop rapidly, they pose a significant forecasting problem for Antarctic coastal areas and maritime areas of southern Australia, New Zealand, South Africa and Chile. In addition, cold-air mesocyclones are an important component of the coupled atmosphere-ocean system: regions experiencing high frequencies of mesocyclones show an associated climatic signature in precipitation, wind speed, and sea level pressure [*Lyons*, 1983; *Bromwich*, 1991; *Sinclair and Cong*, 1992; *Turner et al.*, 1993a; *Carrasco and Bromwich*, 1994; *Carrasco et al.*, 2003]. On decadal and longer time scales, mesocyclones may even help maintain the higher-latitude branch of the thermohaline circulation, as inferred from the close spatial correspondence between mesocyclone maxima in the northern North Atlantic and the downwelling of cold saline water around Greenland and Labrador [e.g., *Harold et al.*, 1999; *Bracegirdle and Gray*, 2008]. A similar relationship may exist in the Antarctic, where coastal polynyas generated or enhanced by strong katabatic winds, participate in the formation of Antarctic bottom water. At least some of those polynya-katabatic wind confluence areas have been noted to coincide with high frequencies of cold-air mesocyclones [e.g., *Carleton*, 1992, 2003]. Recently, *Condron et al.* [2008] have shown that a better representation of polar mesocyclones in ERA-40 reanalyses [*Simmons and Gibson*, 2000] would increase Greenland Sea deep water formation by up to 20% in 1 month. Studies such as these point to the real need to accurately represent mesocyclones in oceanic and coupled climate models, so as to capture the high rates of ocean heat loss otherwise omitted for deep water formation regions.

[5] Accordingly, it is highly desirable to better understand and improve the predictability of time periods and locations of cold-air mesocyclogenesis. Because these systems usually develop within favorable large-scale meteorological environments, especially cold-air outbreaks and PVA [e.g., *Harrold and Browning*, 1969; *Mansfield*, 1974; *Rasmussen*, 1979; *Businger and Reed*, 1989; *Hewson et al.*, 2000; *Claud et al.*, 1992a, 1992b, 1993, 2004], a useful first step toward the aforementioned goal has been to determine the typical (e.g., via composite averaging) regional-scale fields of meteorological variables associated with mesocyclones [e.g., *Businger*, 1985, 1987; *Fitch and Carleton*, 1992; *Carleton and Fitch*, 1993; *Turner and Thomas*, 1994; *Carleton and Song*, 1997; *Carrasco et al.*, 1997a, 1997b; *Claud et al.*, 2007, 2009]. In general, such studies have shown that increased monthly and seasonal frequencies of cold-air mesocyclones coincide with amplified anomalies in 500 hPa height and temperature fields over middle and higher latitudes, either within the anomalous trough or between the trough and the next upstream ridge (i.e., in the region of persistent cold advection) [*Businger*, 1987; *Ese et al.*, 1988; *Fitch and Carleton*, 1992; *Carleton and Fitch*, 1993; *Turner and Thomas*, 1994; *Carleton and Song*, 1997]. The probability of large numbers of mesocyclones increases where and when these conditions coincide with positive anomalies of the sea surface temperature (SST) and near-surface air temperature difference, as well as sea ice extent, such as in the Ross and Bellingshausen/Amundsen seas [e.g., *Carleton and Carpenter*, 1990; *Carleton and Song*, 1997]. These associations suggest the possibility not only of better characterizing areas susceptible to cold-air mesocyclogenesis on monthly to seasonal time scales, but also of improving mesocyclone predictability from consideration of the larger-scale circulation teleconnection patterns within which coupled atmosphere–upper ocean anomalies occur.

[6] Manual interpretation of satellite imagery for mesocyclones, and compositing system frequencies and locations on monthly to seasonal time scales, have revealed preliminary associations with the large-scale atmospheric circulation and teleconnection patterns, particularly El Niño–Southern Oscillation (ENSO) [*Carleton and Carpenter*, 1990; *Carleton and Song*, 1997, 2000]. Although the ENSO has its strongest manifestation in the tropical Pacific, it significantly impacts higher-latitude areas of the SH, particularly the southeast Pacific (see *Turner* [2004] for a review). The most pronounced teleconnection to ENSO occurs as a Rossby wave train having positive (negative) height anomalies over the Amundsen-Bellingshausen Sea during warm (cold) events, and the reverse pattern in the Weddell Sea [*Carleton*, 1988]. Since about 1977, the ENSO has shifted toward a more negative phase of more frequent and stronger El Niño events. However, extratropical climate relationships with ENSO seem not to have been stable even since that time [*Carleton*, 1989; *Bromwich et al.*, 2000], and recent studies [e.g., *Fogt and Bromwich*, 2006; *L'Heureux and Thompson*, 2006] have discussed a possible interdecadal modulation of the ENSO teleconnection in the high-latitude South Pacific by the Southern Annular Mode (SAM). The SAM is the leading mode of atmospheric circulation variations in the SH extratropics [e.g., *Kidson*, 1999; *Limpasuvan and Hartmann*, 1999; *Thompson and Wallace*, 2000; *Carleton*, 2003]. The zonally symmetric structure of the SAM reflects the fact that it is driven by anomalies in the eddy flux of zonal momentum over middle latitudes. During SAM positive (negative) phases, the anomalous poleward flux of eddy momentum drives westerly (easterly) anomalies at 55–60°S [e.g., *Karoly*, 1990; *Limpasuvan and Hartmann*, 2000]. The positive phase of SAM is associated with a strengthening and poleward shift of the storm track over the Southern Ocean [*Thompson and Wallace*, 2000]. In recent years, especially in austral summer and autumn seasons, the SAM has shifted into a more positive phase [*Marshall*, 2003], denoted by a decrease in surface pressure over Antarctica and a strengthening of the westerlies in the coastal region as pressure has risen over middle latitudes [e.g., *Gong and Wang*, 1999; *Renwick*, 2004]. In addition to the ENSO and SAM, zonally asymmetric teleconnections of essentially extratropical origin show important associations with temperature, meridional wind and precipitation for key sectors of the Southern Ocean, the first two variables also being connected to regional anomalies of the Antarctic sea ice [*Harangozo*, 1997]. In particular, the Trans-Polar Index (TPI), typically defined as the Sea Level Pressure (SLP) anomaly difference between Hobart and Stanley [*Pittock*, 1980, 1984; *Rogers and van Loon*, 1982; *Carleton*, 1989, 2003], depicts the eccentricity of wave number one, and has been shown to influence sea ice and mesocyclone distributions in the winter season [*Claud et al.*, 2009]. In its positive (negative) phase, TPI is associated with an enhanced ridge (trough) in the Australian region and an enhanced trough (ridge) in the South American Sector.

[7] Because the few studies relating SH teleconnections and mesocyclone occurrence were generally for short time periods (typically a couple of years representing opposite phases), and utilized data sets on atmospheric and oceanic variables that were considerably less comprehensive than those now available, we revisit this issue specifically for the transition season months. In this paper, we undertake the following sets of analyses: (1) compare previously published inventories of mesocyclones for selected regions to the newly available high-quality long-term meteorological reanalyses to identify typical synoptic atmospheric and upper ocean environments favorable to mesocyclogenesis, and (2) characterize the associations between composite reanalysis meteorological fields associated with mesocyclones and the large-scale circulation patterns of ENSO, SAM and TPI, by deriving maps of enhanced "mesocyclogenesis potential," as well as low probability of mesocyclogenesis, in relation to the extreme phases of those teleconnections. Moreover, because the Antarctic sea ice extent is close to its maximum (minimum) in October (March), an examination of the transition season months permits a fuller assessment of the climatic role of sea ice conditions in mesocyclogenesis over higher southern latitudes compared to the winter season. To the knowledge of the authors, this study is the first to address these issues at a hemispheric scale and by considering simultaneously the ENSO, SAM, and TPI.

[8] The paper is organized as follows. In section 2, we present the data and analysis methods. In section 3, we determine variables useful for identifying areas having high frequencies of cold-air mesocyclones, on the basis of previously published inventories of mesocyclones and the reanalysis fields in transition season months. In section 4, we describe associations between the mesocyclone-significant

variables and large-scale circulation, as revealed by spatial composites of mesocyclone reanalysis variables according to teleconnection phases. From those composite results, in section 5 we identify the spatial areas likely to see enhanced, and also suppressed, formation of mesocyclones relative to background levels on hemispheric scales (the mesocyclogenesis potential). The results and implications of the study are summarized in section 6.

2. Data and Analysis

[9] The transition season months comprise March, April, October, and November (i.e., two adjacent months representing SH autumn and spring, respectively). Individual months rather than 2 month averages are considered because conditions can change markedly between adjacent months (for example, sea ice concentration and extent), and our calculations show that the statistical relationships between teleconnections differ on monthly time scales (see section 4.1). We do not consider the month of September because, although an equinoctial month like March, it retains characteristics of the SH winter season [*van Loon*, 1966, 1967; *Streten and Troup*, 1973; *Carleton*, 1979] resulting from the temporal lag between insolation minimum and lowest air temperatures over higher southern latitudes. For example, in most years, the sea ice continues to expand equatorward during September. Accordingly, we included September in our recent study of mesocyclone-circulation teleconnection associations for the winter season [*Claud et al.*, 2009]. The month of May was not considered because there is no mesocyclone inventory available for this month.

2.1. Mesocyclone Inventories

[10] Although there exists a number of long-term climatologies of extratropical cyclone tracks based on reanalyses, they cannot be used for our purpose. For the Northern Hemisphere, *Condron et al.* [2006] compared satellite-based with reanalysis-based cyclone climatologies, and showed that about three out of every four systems having a size between 100 and 500 km were not reproduced in ERA-40. It is, therefore, necessary to rely on satellite-based climatologies. Unfortunately, and unlike for the winter season, these satellite-based mesocyclone inventories are few in number for the SH in the transition season months. However, to help guide our choice of meteorological variables with which to depict cold-air mesocyclone environments, we used the inventories for individual transition season months given by *Fitch and Carleton* [1992] and *Carleton and Song* [1997] (which include both single-banded mesocyclones evident initially in satellite images as enhanced convection in cold-air masses (i.e., "comma cloud") and multibanded ("spiraliform") types). Therefore, in the following analysis, we compare monthly averages of the mapped reanalyses fields with mesocyclone locations derived separately for (1) March, April, and October 1988 and centered on the "half-hemisphere" between approximate longitudes 100°E eastward to 50°W [*Fitch and Carleton*, 1992, hereafter FC92] and (2) March–April and October–November 1992 in the Australasian sector (70°E–150°W) [*Carleton and Song*, 1997, hereafter CS97]. The years studied represent large variations in SH atmospheric circulation, including a transition from El Niño to La Niña (1988), and a prolonged El Niño that began in 1991 [*Cullather et al.*, 1996; *Trenberth and Hoar*, 1996]. To complement this investigation, we also consider a partial (sample) census of mesocyclones undertaken for March and April 1990 which, unlike the previous inventories, is available for the full SH poleward of 45°S (Figure 1).

[11] In the FC92 study, as for the period March–April 1990, mesocyclones were identified on the basis of visual interpretation of twice-daily medium resolution (5.4 km^2) thermal infrared hard-copy images acquired by the polar-orbiting Defense Meteorological Satellite Program (DMSP). The spatial and temporal resolutions of the DMSP imagery are unlikely to have significantly biased the detection of mesocyclones because shorter-lived systems also tend to be weaker, and most mesocyclones are evident at the 5.4 km^2 resolution used on the half-hemispheric mosaics [e.g., *Carleton*, 1987]. Further details on the DMSP imagery used to derive mesocyclone inventories are given by *Carleton and Carpenter* [1990] and CF93.

[12] In the CS97 study, mesocyclones were identified using geosynchronous GMS (Geostationary Meteorological Satellite) images. Although these are less advantageous than the polar-orbiting DMSP owing to the large satellite viewing angles for the higher latitudes, their use was facilitated by rectifying raw images to a polar stereographic format, thereby improving the ability to detect mesocyclones. Also, CS97 noted that most larger mesocyclones over sea ice (for October, November) and ocean areas (all months) were likely to have been captured in the analysis of rectified images.

2.2. Long-Term High-Resolution Reanalyses

[13] Meteorological data are available as reanalyses generated by a numerical forecast model that assimilates available observations. Among those, the ERA-40 data assimilation system [*Simmons and Gibson*, 2000] uses the Integrated Forecasting System (IFS) developed jointly by ECMWF and Météo-France. A three-dimensional variational method assimilates the observations into the model, which has 60 vertical levels and T159 horizontal spectral resolution. Data are available since 1957 for 23 pressure levels with a spatial resolution of approximately 125 km (1.125°). A detailed description of the ERA-40 data set can be obtained at http://www.ecmwf.int/research/era. Since 1979, the reanalysis makes comprehensive use of satellite observations; before then, the atmospheric fields over higher southern latitudes are model-dominated. Hence, to avoid possible discontinuities due to the inclusion of satellite data [e.g., *Bromwich and Fogt*, 2004; *Sterl*, 2004], we study the period 1979–2001.

[14] Despite the availability of monthly ERA-40 SST, we utilize the Extended Reconstructed Sea Surface Temperatures (ERSST), which correspond to a monthly extended reconstruction of global SST based on the Comprehensive Ocean-Atmosphere Data Set and uses sea ice concentrations to improve the high-latitude SST analysis [*Smith and Reynolds*, 2003, 2004]. The ERSSTs have undergone stringent quality control, and are available at the following address: http://lwf.ncdc.noaa.gov/oa/climate/research/sst/sst.html#ersst. Sea ice concentrations retrieved from passive microwave radiances of the NIMBUS-7 SSMR and DMSP SSM/I are obtained from http://nsidc.org/data/seaice_index/ [*Cavalieri et al.*, 1996]. Both the sea ice concentration and

Table 1. List of Years Considered for Producing the Composites[a]

	Niño Year$_0$	Niña Year$_0$	TPI+	TPI−	SAM+	SAM−
March	1983, 1987, 1992, 1995, 1998	1985, 1989, 1996, 1999, 2000	1985, 1988, 1993, 1994	1979, 1984, 1997, 1999	1979, 1982, 1994, 1996, 1997	1980, 1981, 1986, 1988, 1999
April	1983, 1987, 1992, 1995, 1998	1985, 1989, 1996, 1999, 2000	1985, 1987, 1988, 1989, 2001	1979, 1981, 1995, 1998	1982, 1988, 1998, 1999, 2001	1980, 1981, 1990, 1991
October	1982, 1986, 1991, 1994, 1997	1984, 1988, 1995, 1998, 1999	1982, 1984, 1990, 1992	1986, 1988, 1989, 2001	1983, 1991, 1996, 1999, 2001	1982, 1988, 1995, 1997
November	1982, 1986, 1991, 1994, 1997	1984, 1988, 1995, 1998, 1999	1986, 1988, 1989 1990, 2000	1987, 1991, 1994	1981, 1983, 1985, 1998, 1999, 2001	1979, 1980, 1982, 1994, 1996, 1997, 2000

[a]TPI, Trans-Polar Index; SAM, Southern Annular Mode.

SST data have been regridded onto the ERA-40 grid of 1.125° spatial resolution to make all fields compatible.

2.3. Statistical Analysis

[15] To characterize the associations between large-scale teleconnection patterns and mesocyclone environments, we perform temporal linear intercorrelations of teleconnection indices and derive spatial composites of the atmospheric reanalysis fields. The monthly indices for ENSO and TPI were acquired from http://www.cdc.noaa.gov/gcos_wgsp/, and for SAM from http://www.antarctica.ac.uk/met/gjma/sam.html. Because the peak in most ENSO indices typically occurs in the SH summer, we use a seasonal index calculated by averaging the normalized Niño 3.4 SST index [*Trenberth*, 1997] over the broad seasonal period October through February. In addition, we compute correlations and spatial composites for ENSO opposite phases (El Niño, La Niña) both in year 0 and the term 12 months earlier (year − 1). Previous studies [e.g., *van Loon*, 1984; *van Loon and Shea*, 1985; *Carleton*, 1988, 2003] have indicated large changes in SLP and other climatic indices (e.g., sea-ice concentration) over SH middle and higher latitudes between ENSO year 0 and year − 1, particularly for El Niño. For autumn months (March–April), year 0 immediately follows the peak in the index while for spring months (October–November), year 0 represents the onset year. Thus, in the composites, autumn (year − 1) precedes spring (year 0) by a half year, as does spring (year − 1) with respect to autumn (year − 1).

[16] For each month and teleconnection considered, only the extreme years have been selected for determining the composites. This is a standard procedure in composite analysis as it avoids the noise that can be introduced by including near-neutral years. Depending on the month and teleconnection considered (Table 1), the number of years for producing composites ranges from 3 (November, TPI negative) to 7 (November, SAM negative), with a majority comprising 4 or 5 years.

[17] The statistical significance of the composites is assessed at each grid point using a phase-scrambling bootstrap test with 999 samples [*Davison and Hinkley*, 1997], taking into account the autocorrelation characteristics of each time series.

3. Mesocyclone Spatial Distributions: Associated Surface and Atmospheric Fields

[18] In *Claud et al.*'s [2009] study for the SH winter-season months, mesocyclone frequencies over the open ocean were found to increase when and where the difference between the SST and the temperature at 925 hPa (SST-T925) increases, in conjunction with south to southwesterly low-level (925 hPa) winds (**V**925). These associations suggested strong upward fluxes of heat and moisture, particularly west and southwest of midtropospheric troughs and frontal cyclones. Additional favorable conditions for mesocyclones include negative anomalies of temperature at 500 hPa (T500), typically accompanied by greater sea ice extent in those longitudes [e.g., *Yuan et al.*, 1999]. Conversely, unfavorable conditions for mesocyclone development involve negative or only weakly positive SST-T925; low-level winds having northerly components (i.e., a stable lower atmosphere); warm air at 500 hPa; and reduced sea ice extent (i.e., implied downward fluxes of heat typically located east of frontal cyclones and west of high-pressure ridges [*Carleton and Carpenter*, 1989]). To determine the extent to which these variables are important for mesocyclogenesis in the transition season months, we identify their associations with the first satellite observation of each mesocyclone given in the inventories, at the daily level (Table 2). The percentages of mesocyclogenesis associated with a large positive SST-T925 (second column), low T500 (third column), or southerly **V**925 (fourth column) are stratified by month considered. A threshold of 6K (10K) was used for SST-T925 in the months of March and April (October and November). There is no unique threshold value for T500 because of the latitude dependence. The analysis is restricted to latitudes poleward of 45°S (in the 1992 inventory, mesocyclones were reported at latitudes lower than 45°S). Among the three variables, the more robust association is with T500 (Table 2). Mesocyclogenesis is most frequently associated with low T500 (74% of cases, on average). In addition, there is relatively little variation

Table 2. Percentages of Mesocyclones Associated With ERA-40 Daily Fields of Large SST-T925, Low T500, and a Southerly **V**925 Component, for Each Transition Season Month Considered[a]

Months	Large SST-T925	Low T500	**V**925 With a Southerly Component
March 1988 (37)	70	81	49
April 1988 (53)	70	68	75.5
October 1988 (50)	56	74	60
March 1992 (47)	62	74.5	51
April 1992 (51)	68.5	72.5	61
October 1992 (59)	64.5	81	60
November 1992 (51)	45	67	56
March 1990 (14)	50	71	50
April 1990 (16)	62.5	75	56

[a]The total number of mesocyclones in each month is given in parentheses.

Table 3a. Correlation Coefficients of Teleconnection Indices for Transition Season Months and Over Different Time Periods[a]

		SAM			
TPI	Period	March	April	October	November
March	1979–2001	0.09	0.04	−0.20	0.12
	1957–1978	0.16	**0.34**	−0.14	−0.22
April	1979–2001	−0.03	0.10	−0.04	0.06
	1957–1978	0.14	0.19	**0.36**	**0.53**
October	1979–2001	**0.33**	−0.29	0.17	−0.16
	1957–1978	−0.04	**−0.36**	**0.37**	**0.38**
November	1979–2001	−0.30	0.08	−0.10	0.28
	1957–1978	0.04	−0.11	**0.60**	**0.79**

[a]Transition season months are March–April and October–November. Values in bold are significant at the 90% confidence level.

of percentages among the months or periods considered (68–81%). Practically all the remaining cases were first observed in association with large T500 gradients, mostly to the west of troughs. Mesocyclogenesis frequencies of about 60%, on average, are associated with southerly **V**925 and also large SST-T925, although there are large variations from one month/region to another (values range between 49 and 75.5% for **V**925, and 45–70% for SST-T925). In addition, for most cases when the meridional component of **V**925 was not from the south, the zonal component of **V**925 was large; that is, cold-air mesocyclones are associated with either southerly winds or strong westerly winds. Specifically for the variable SST-T925, a large number of mesocyclones formed in areas where the horizontal gradient is large.

[19] The results presented in Table 2 confirm those for the winter season [*Claud et al.*, 2009]. Mesocyclones occur preferentially in association with either low temperatures at 500 hPa or proximity to large gradients of T500. Additional favorable conditions for mesocyclones are confirmed to include a large positive difference in SST-T925, coincident with south to southwesterly low-level winds (**V**925). An increase of mesocyclones along the sea ice edge (especially in October) [see also *Carleton and Fitch*, 1993; *Carleton*, 1995; *Carleton and Song*, 2000], and an association with preferred areas for katabatic winds near the Antarctic coast (the Ross Sea or Adelie Land; March and April 1988) was also noted. Conversely, unfavorable conditions for mesocyclone development (i.e., reduced frequencies of vortices) generally involve negative or only weakly positive SST-T925; low-level winds having northerly components (i.e., a stable lower atmosphere); and warm air at 500 hPa.

4. Composite Patterns of Reanalysis Fields Associated With Teleconnections

4.1. Teleconnection Statistical Interrelationships

[20] Updated [cf. *Carleton*, 1989] intercorrelations between the teleconnection indices (SAM, ENSO, and TPI) for transition season months (March–April and October–November) are presented in Tables 3a and 3b. A number of studies suggest a change in statistical correlation between the ENSO and Antarctic-region climate variables between the 1980s and 1990s (e.g., for precipitation [*Fogt and Bromwich*, 2006; *Thomas et al.*, 2008]). To check whether the intercorrelations are consistent within the recent period, we calculate these separately for 1979–1990 (i.e., first subset of the recent period) and 1991–2000 (second subset). In addition, and for comparison purposes, we calculate correlations for the earlier period 1957–1978.

[21] For the full recent period 1979–2001 (Table 3a), TPI and SAM were not significantly correlated at the 90% level, except SAM in March with TPI in October (correlation of 0.33). By contrast, for 1957–1978, correlations between TPI and SAM generally were larger and more significant, especially for the spring. For 1979–2001, SAM and ENSO (year − 1) were significantly related only in November at r = 0.33 (Table 3b). When considering SAM and ENSO at year 0, a positive correlation is obtained in March (0.56) and a negative one is obtained during spring (−0.57 in October and −0.4 in November). Changes are evident in the correlations between the two recent subperiods (1979–1990 and 1991–2000), with absolute values being generally larger for the latter period. The increase in the 1990s of the correlations for austral spring is consistent with previous findings [*Fogt and Bromwich*, 2006; *L'Heureux and Thompson*, 2006].

[22] The TPI and ENSO (year − 1) in the period 1979–2001 are not significantly correlated. Moreover, the TPI and ENSO at year0 are only significantly negatively correlated in November (−0.37). As was noted with regard to the SAM, these teleconnection inter-correlations generally are not stable on decadal timescales, with even a sign reversal evident between the two sub-periods, particularly in autumn.

[23] For the earlier period 1957–1978, TPI and ENSO were significantly correlated during spring months, at year 0 but not at year − 1. The SAM and ENSO were significantly positively correlated during spring at year − 1 and negatively in April at year 0.

[24] The foregoing results confirm the lack of stability in the correlations between teleconnection indices at decadal and multidecadal scales for transition season months. Because the period we are considering for the synoptic composites associated with mesocyclones is rather short

Table 3b. Correlation Coefficients of Teleconnection Indices for Transition Season Months and Over Different Time Periods[a]

	1956–1977	1978–2000	1979–1990	1991–2000
	Niño, Year 0			
SAM March	−0.17	**0.56**	**0.58**	**0.64**
SAM April	**−0.49**	−0.24	0.06	**−0.71**
SAM October	−0.24	**−0.57**	0.17	−0.48
SAM November	0.02	**−0.40**	**−0.50**	**−0.66**
TPI March	−0.11	0.00	−0.03	0.03
TPI April	−0.23	0.07	−0.37	**0.59**
TPI October	**0.36**	0.11	0.12	0.10
TPI November	**−0.36**	**−0.37**	−0.18	**−0.60**
	Niño, Year − 1			
SAM March	0.30	−0.21	−0.11	**−0.47**
SAM April	0.09	0.30	0.28	0.28
SAM October	**0.37**	−0.22	−0.04	**−0.51**
SAM November	**0.33**	**0.33**	0.31	0.37
TPI March	0.16	−0.33	**−0.56**	−0.03
TPI April	0.15	0.01	−0.03	0.10
TPI October	0.12	0.25	0.05	**0.50**
TPI November	0.13	−0.30	−0.31	−0.29

[a]Transition season months are March–April and October–November. Values in bold are significant at the 90% confidence level.

(1979–2001), caution should be exercised when interpreting results for the months and teleconnections that are significantly correlated (see discussion in section 5).

4.2. Composites

[25] The associations between polar mesocyclones and teleconnections are inferred from the composite anomaly fields of SST-T925, the wind at 925 hPa (**V**925), and T(500) (Figures 3–8). We first discuss the patterns for spring because these precede the peak in ENSO (year 0), they pertain to the time around (October) or just after (November) the maximum sea-ice extent, and they follow sequentially the patterns for the winter season (June–September) presented by *Claud et al.* [2009]. Each of the three large-scale teleconnections is discussed successively, emphasizing the months and patterns that show the largest statistically significant associations. To make more apparent the large-scale associations, we show composite standardized anomalies relative to the 1979–2001 mean fields that are displayed in Figure 2 for each of the four autumn and spring months. Unless specified, only results significant at the 90% confidence level are discussed. Only a few mapped composites are shown (Figures 3–8), but they are synthesized in section 5 with an index of mesocyclogenesis activity, the mesocyclogenesis potential, for October and March.

4.2.1. Spring (October–November)

[26] In the spring of the ENSO onset year (i.e., year 0, Figures 3a and 3c), a significant signal in SST-T925 and **V**925 is observed, particularly for the anticyclonic circulation anomaly (indicated by **V**925) in the southern Pacific Ocean in October. Because this feature has associated anomalies in SST-T925 and in T500, there are expected to be consequences for mesocyclone formation: conditions are deemed favorable for mesocyclogenesis over the eastern part of the Bellingshausen Sea and to the southeast of New Zealand, but unfavorable over the Amundsen Sea. The results are opposite for La Niña years (Figures 3b and 3d), which is consistent with the composite circulation changes noted in previous studies [e.g., *van Loon and Shea*, 1985; *Carleton*, 1988]. In November (Figures 3e–3h), the El Niño (year 0) has associated positive anomalies of SST-T925, southerly winds, and lower 500 hPa temperatures in the sector 110–150°E, and to the north of the Weddell Sea. Accordingly, these two regions are likely to see increased frequencies of mesocyclones. By contrast, La Niña years likely see more mesocyclone activity equatorward of the sea ice edge at around 65°S, between 150°E and 150°W. Associations between ENSO at year − 1 and SST-T925, **V**925 and T500 (not shown) are much weaker compared to year 0, especially in October.

[27] Associations between the SAM and near-surface climate conditions are stronger in the negative phase than in the positive phase, both in October (Figures 4a–4d) and November (Figures 4e–4h). In October, during negative SAM, the formation of mesocyclones is expected to be favored along the sea ice edge, especially northeast of the Weddell Sea, yet inhibited over the area 90°–120°E (Figures 4b and 4d). In November (negative SAM), mesocyclone development should increase relative to background levels practically everywhere except north of the Ross Sea. As is also observed for March (see below), the SAM positive phase in October shows practically no significant association with SST-T925 and **V**925. Associations are somewhat stronger for **V**925 in November, with significantly increased westerlies over the area 60°–70°S from 10°W to 110°W. In November, for positive SAM, negative T500 anomalies prevail over the Antarctic continent and the Ross and Amundsen Seas, while the situation is reversed there for negative SAM.

[28] For the positive TPI in October (not shown), the Bellingshausen Sea and part of the Amundsen Sea should see more mesocyclone activity, given negative T500 anomalies and southerly anomalies of **V**925 in that region. Similarly, over the area between about 150°E and 180°, SST-T925 anomalies are significantly positive, **V**925 southerly anomalies prevail, and T500 anomalies are negative, while at about 180° longitude apart, the opposite results are observed, the latter implying reductions in mesocyclone activity. A positive TPI phase in November (not shown) is likely to be associated with less mesocyclone activity practically everywhere, owing to significant negative SST-T925 and positive T500 anomalies (the composites in **V**925 are almost never significant). When TPI is negative for both October and November, a large area centered on Drake Passage displays significantly negative SST-T925 anomalies, northerly **V**925 anomalies and positive T500 anomalies, all unfavorable for mesocyclogenesis.

4.2.2. Autumn (March–April)

[29] For ENSO (year 0) in March (i.e., a few months after the peak of El Niño; see Table 1), positive SST-T925 anomalies coincident with southerly wind anomalies occur on both sides of the Antarctic Peninsula (barely significant), and also centered near 150°E (Figure 5). Because these low-level anomalies co-occur with negative T500 anomalies, mesocyclogenesis is particularly favored. The opposite pattern (and implied suppression of mesocyclogenesis) occurs in the Ross Sea and western Amundsen Sea. This situation contrasts with that for La Niña events, during which the Weddell Sea and the region just west of the Antarctic Peninsula should see fewer mesocyclones because northerly winds blow over negative SST-T925 values, while part of the Ross Sea should see more activity owing to southerly wind anomalies and more positive SST-T925. Associations between ENSO and **V**925 are rather small in April year 0 (not shown), with only small regions characterized by significant anomalies of positive SST-T925 and negative T500.

[30] For April in ENSO year − 1 (Figure 6), associations with mesocyclone development are stronger than they are in March (not shown). In particular, for Niño years, an anticyclonic circulation anomaly appears in the southern Pacific Ocean between 140° and 180°W: northerly wind anomalies, a reduced vertical temperature gradient and positive T500 anomalies prevail, all considered unfavorable for mesocyclogenesis. This situation contrasts with that for the area east of 120°W. La Niña events are mostly associated with negative SST-T925 anomalies, coincident with northerly wind anomalies and generally positive T500 anomalies (i.e., unfavorable climatically for mesocyclogenesis) at three locations: between 60° and 100°E, north of the Ross Sea and both sides of the Drake Passage.

[31] For March, the association between a positive SAM phase and mesocyclone activity is observed only for small areas (not shown), however, the association is stronger for

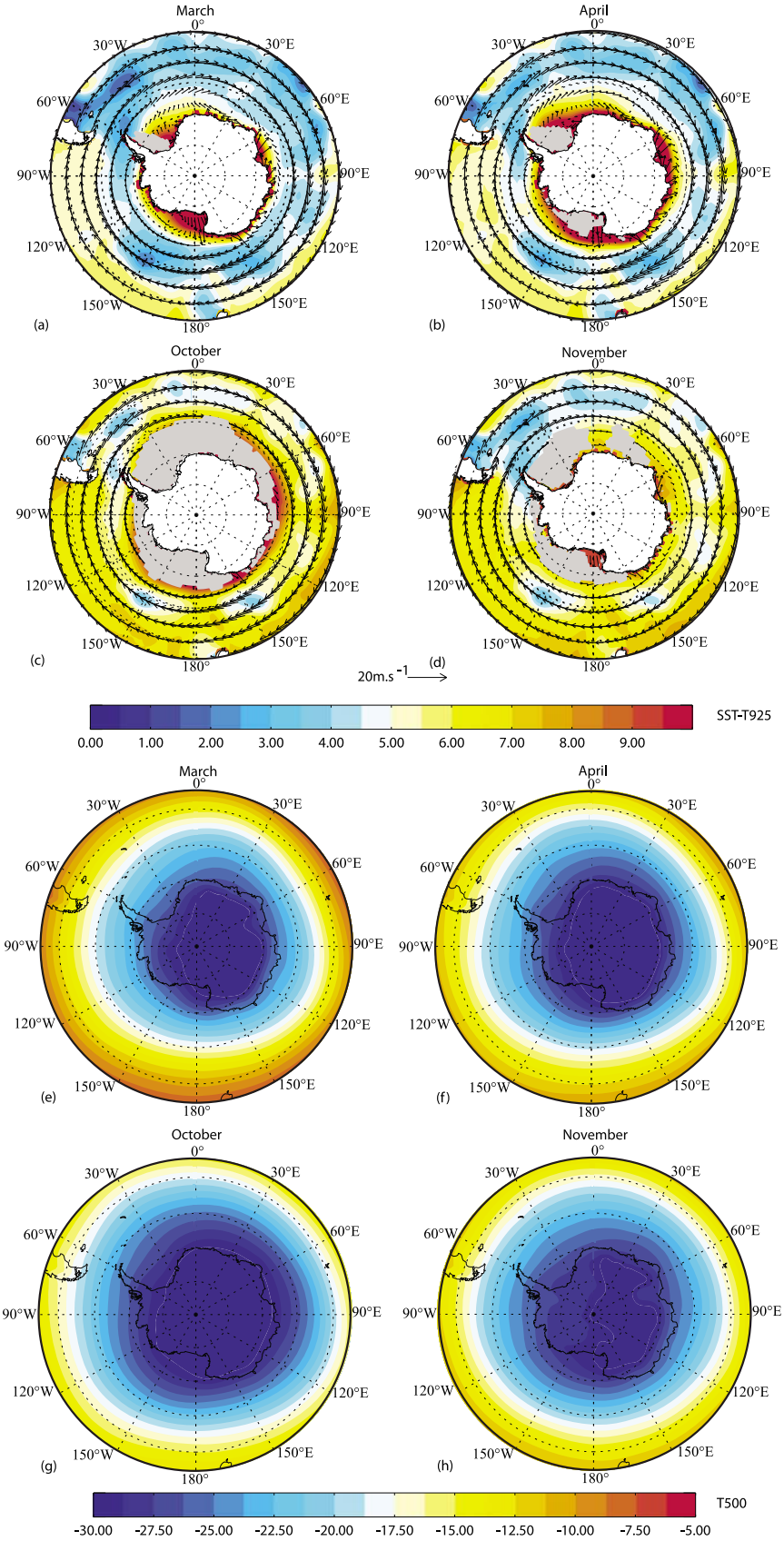

Figure 2. Monthly mean values of wind vector at 925 hPa (**V**925, m/s) and difference between SST and temperature at 925 hPa (T925, K) for the period 1979–2001 for (a) March, (b) April, (c) October, and (d) November. Corresponding temperatures at 500 hPa (T500, K) for (e) March, (f) April, (g) October, and (h) November.

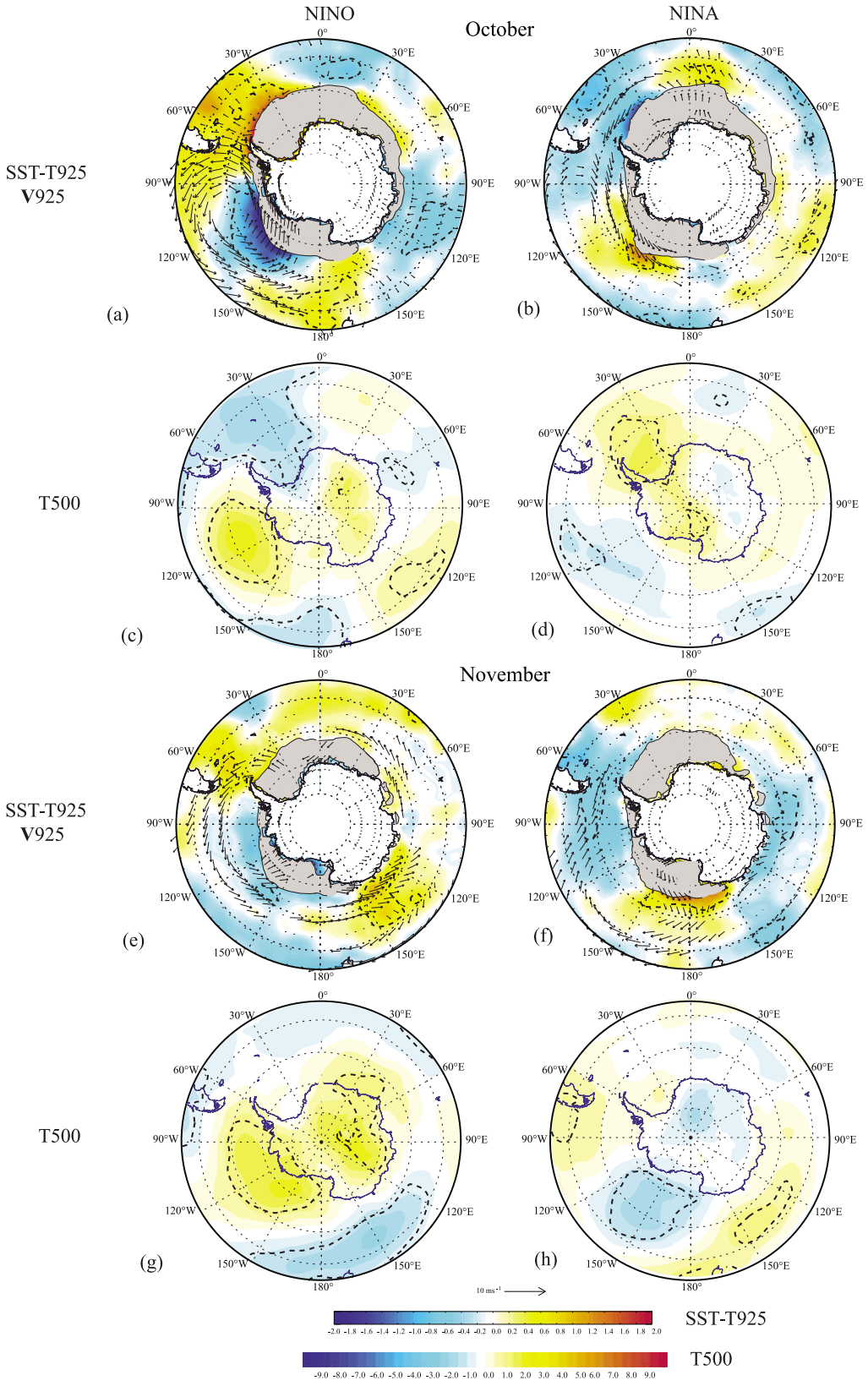

Figure 3. Composite standardized anomalies of the difference SST-T925 and **V**925 with respect to El Niño and La Niña events, and T500 for (a–d) October of year 0 and (e–h) November of year 0. Only anomalies of **V**925 corresponding to a 90% confidence level following a phase-scrambling procedure with 999 samples are plotted (see text for more details). For SST-T925 and T500 anomalies, the 90% confidence level is superimposed (dashed line). Grey areas correspond to grid points where at least one SST monthly value used to construct the composites was set to "undefined" because of land or sea ice.

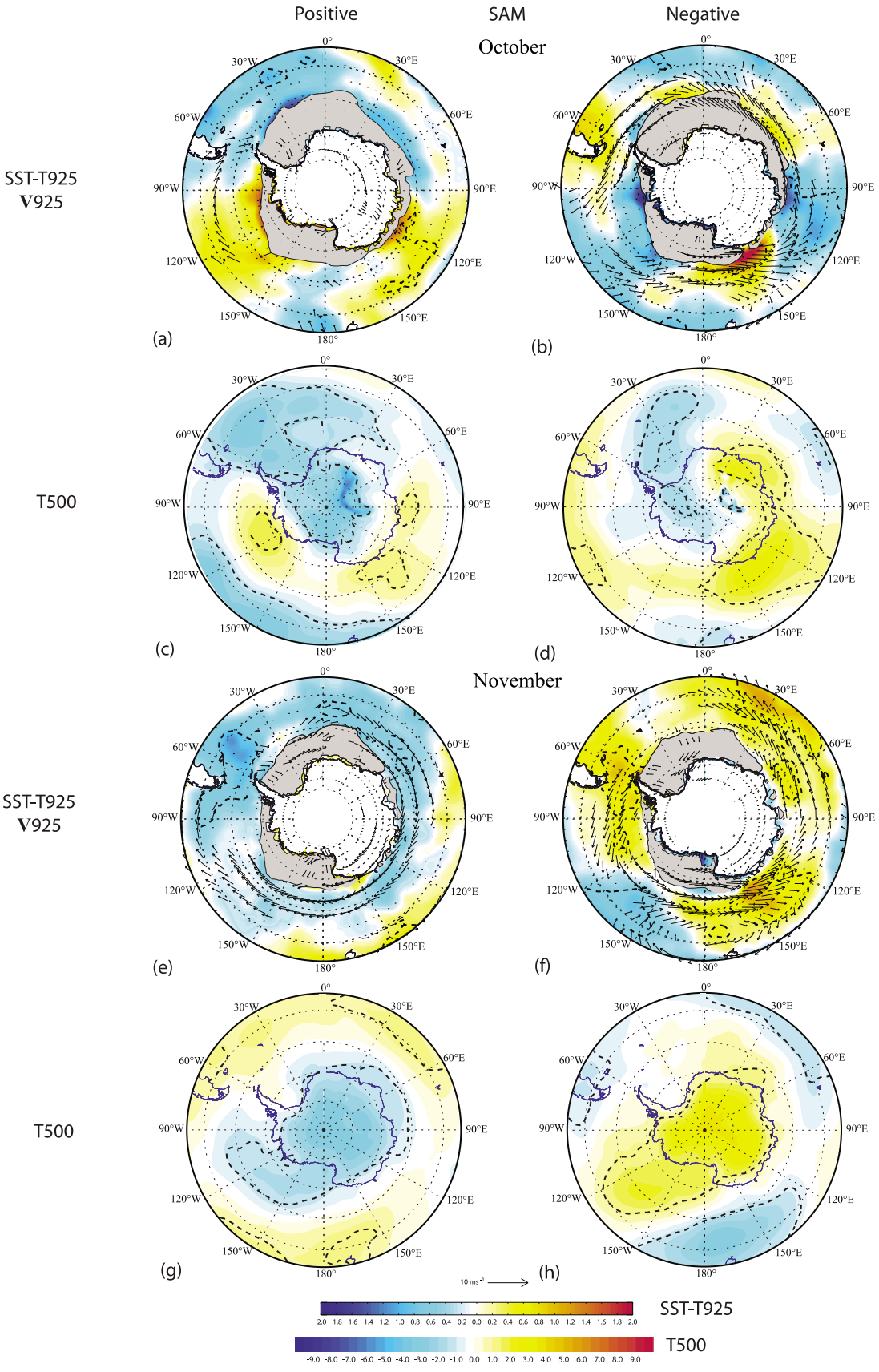

Figure 4. Similar to Figures 3a–3h but for SAM.

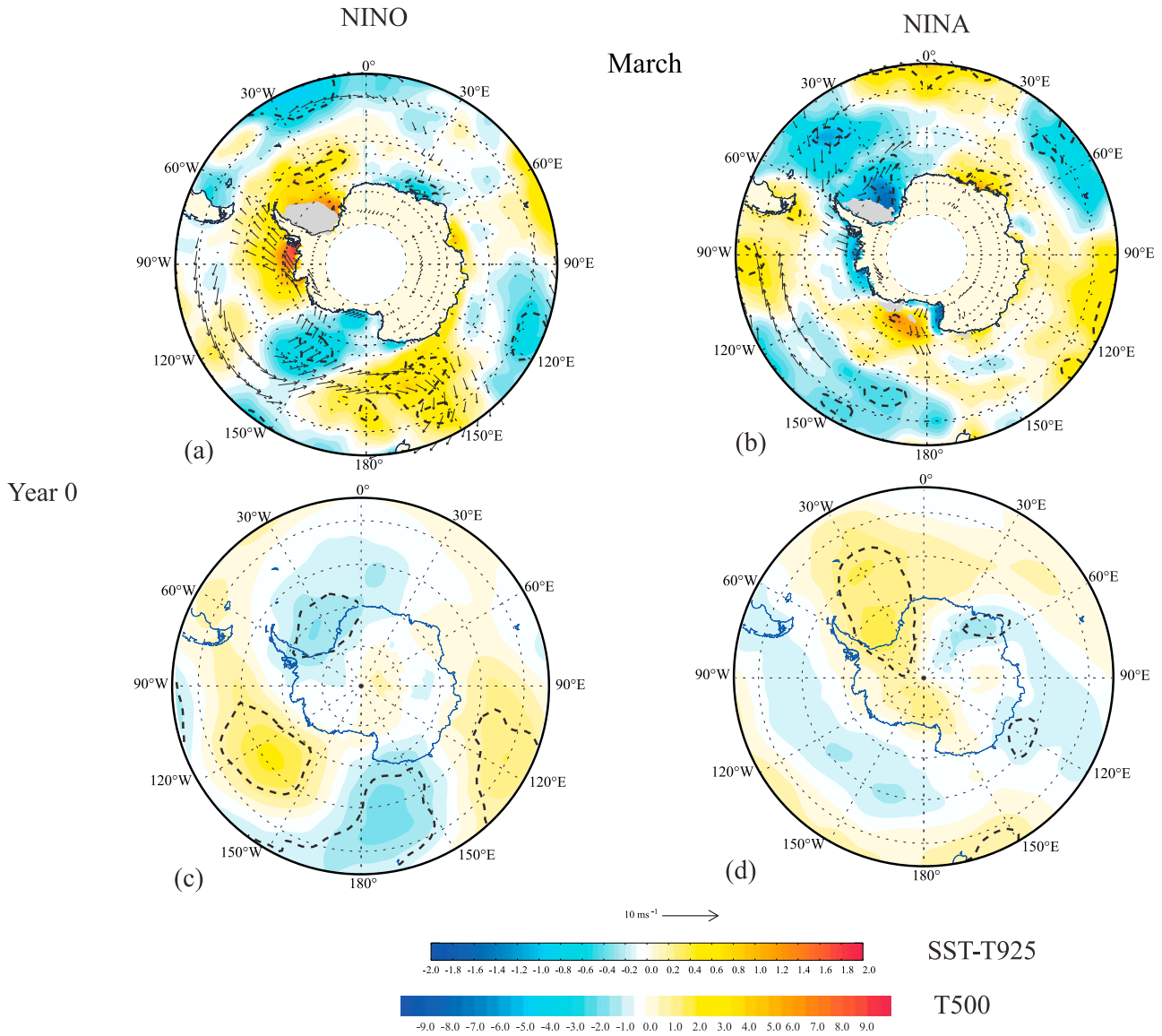

Figure 5. Similar to Figures 3a–3d but for March.

the negative phase (not shown) with three areas displaying positive SST-T925 anomalies (at 150°E, 60°E, and 30°W). These areas also correspond to negative T500 anomalies and, in certain locations, southerly **V**925 anomalies, all of which suggest increased mesocyclone activity over the three ocean basins in the SAM negative phase. In April, a SAM negative phase likely sees more mesocyclones in the Drake Passage area, over the region between 10°W and 6°E, and at about 60°S, 180°; all areas having positive SST-T925 anomalies, southerly **V**925 anomalies and negative T500 anomalies. By contrast, a lack of mesocyclones is expected over most of the Amundsen Sea and along the Antarctic coastline for longitudes 90°–150°E. For the SAM positive phase in April (Figures 8a–8d), the anomalies are statistically significant over larger areas compared to March. Because these are mostly negative SST-T925, northerly **V**925 and warmer T500, the expectation is for fewer mesocyclones. One exception is along the Antarctic coastline, between longitudes 60°–120°E.

[32] For the TPI positive phase in March (Figure 7), the area between 150°E and 180° is expected to see more mesocyclones given the presence of positive SST-T925, southerly winds, and low T500 anomalies. For three locations (between 50° and 60°S for longitudes 120°W to 150°W; closer to the Antarctic continent, between 90°E and 120°E, and at around 0° longitude), fewer mesocyclones should develop because of negative SST-T925, wind anomalies having a northerly component; and T500 positive anomalies. The latter situation contrasts with that for negative TPI, for which mesocyclone formation is favored away from the continent at around 150°W, 30°W, and to a lesser extent near 120°E. The area between 150°E and 180° should see a dearth of mesocyclones, along with the Bellingshausen and Admundsen seas. Similar alternating patterns are observed for positive TPI in April (Figure 8), even though the association is somewhat less marked. For positive TPI, an increase in mesocyclone activity is expected between 120°–150°W, and for relatively low latitudes, between 30° and 60°E and 120° and 150°E, because of

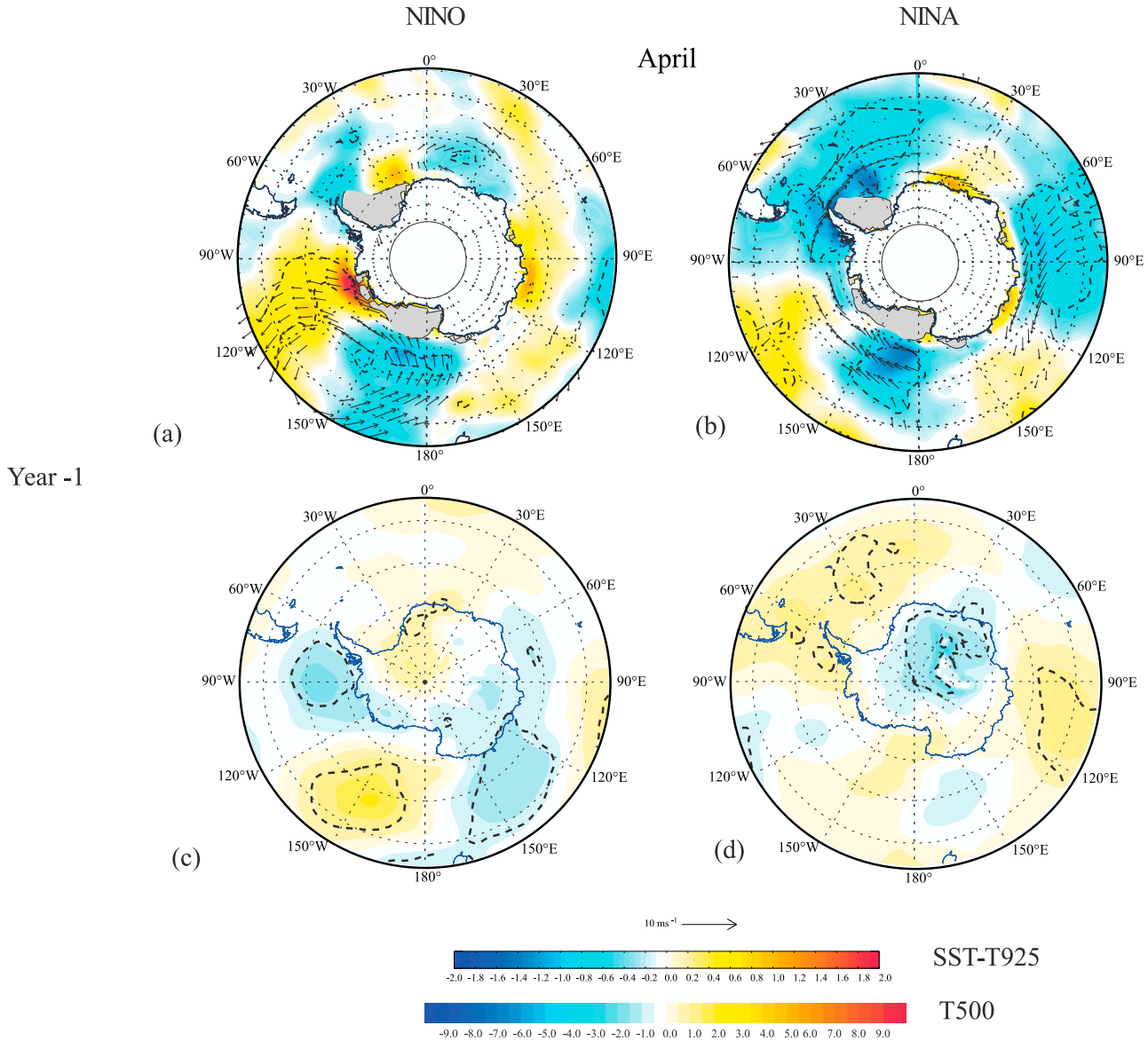

Figure 6. Similar to Figure 5 but for April and year − 1.

the presence of positive SST-T925, wind anomalies having a northerly component, and negative T500 anomalies. In between those areas, fewer mesocyclones are expected, especially southwest of New Zealand and in the Bellingshausen Sea because unfavorable upper ocean and atmospheric conditions prevail.

5. Mesocyclogenesis Potential for Teleconnection Phases

[33] To depict the spatial areas favorable, and also unfavorable, to mesocyclogenesis for different teleconnections, it is necessary to integrate the important information from each reanalysis composite map. We achieve this objective by applying the "mesocyclogenesis potential" (MCP) method we previously developed for the winter season [*Claud et al.*, 2009], to the spring and autumn months. The MCP denotes the increase in mesocyclone-favorable conditions relative to background activity for a given month, according to four nominal categories of elevated probability: "Increased," "Moderate," "High," and "Maximum." These categories are determined from the spatial coincidence of overlapping areas for the following mesocyclone-favorable conditions: negative anomalies of T500; positive values of SST-T925; anomalies of **V**925 having a southerly component; and location within 2.5° latitude of the sea-ice edge [*Carleton and Fitch*, 1993] or continental ice margin under off-ice airflow conditions. The four MCP categories are defined as follows: (1) Increased Probability: any one favorable condition present, or two favorable conditions present along with a mesocyclogenesis unfavorable condition (see below); (2) Moderate Probability: any two favorable conditions co-occurring; (3) High Probability: all but one favorable condition present; and (4) Maximum Probability: all four mesocyclone-favorable conditions present (i.e., southerly winds coinciding with positive SST-T925, location beneath negative T500 anomalies, and proximity to the sea ice or land ice edge).

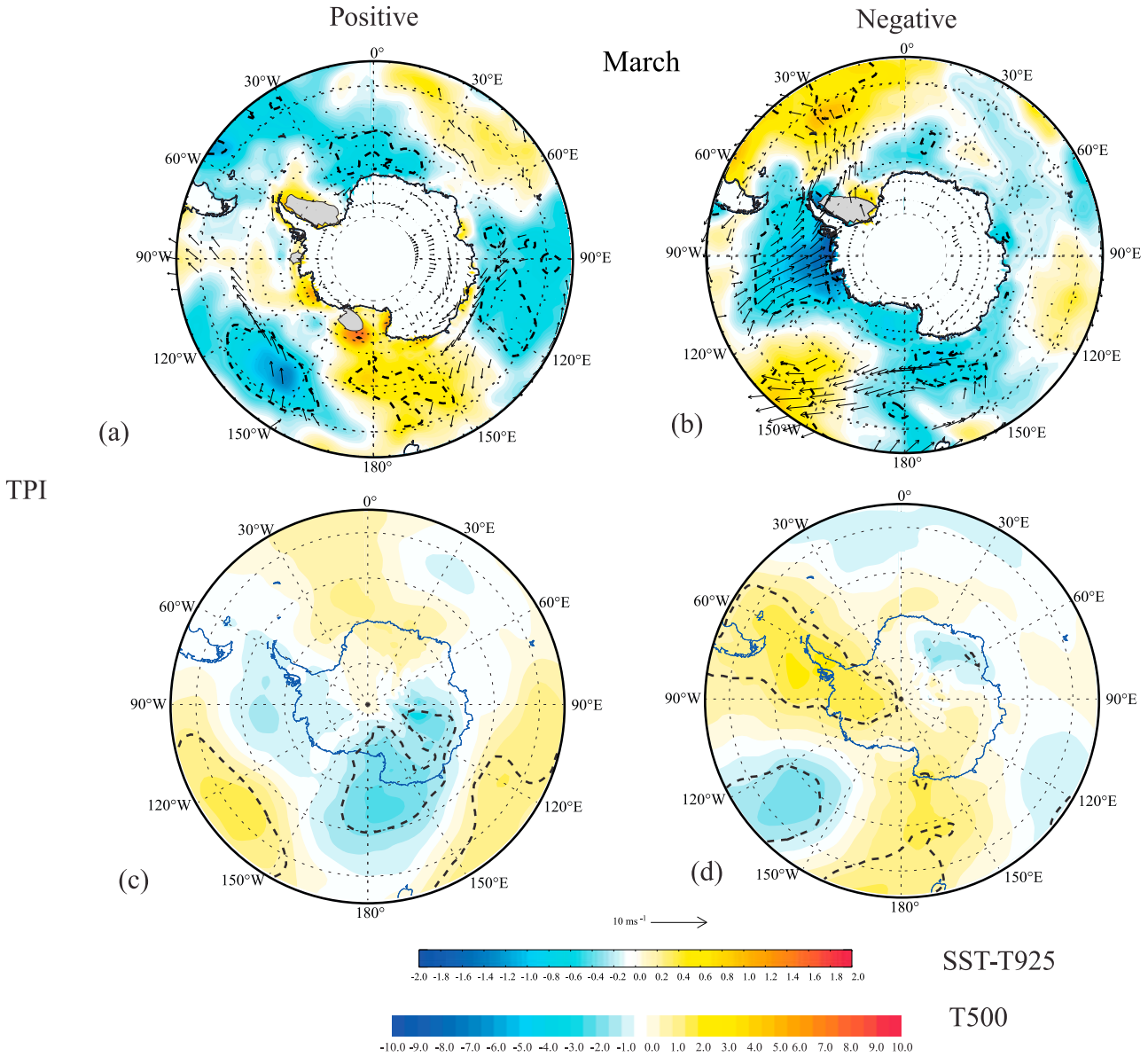

Figure 7. Similar to Figure 5 but for March and TPI.

[34] In determining MCP categories by teleconnection phase, the spatial areas identified for each reanalysis variable (T500, SST-T925, **V**925) are contained within the 90 percent confidence level of the composite, and extend into adjacent areas having large differences of the same sign. The MCP is not determined over the Antarctic continent or ice shelves, or for sea-ice-covered areas, because one or more mesocyclone-relevant variables are either absent or have little physical meaning (e.g., SST-T925). This consideration is particularly important in October because of the typically large areal extent of sea ice in that month. The MCP method currently does not weight regional differences in mesocyclone formation factors, such as the important role of katabatic winds in the western Ross Sea or a dominant upper cold pool of air in the Amundsen and Bellingshausen seas [cf. FC92; *Carleton and Fitch*, 1993]. Future refinement of the method to account for such regional differences is desirable. Notwithstanding, the generation of unweighted MCP monthly summary maps (Figures 10–13, discussed below) readily permits intrahemispheric comparisons of the locations and areal coverage of each category; for opposite phases of the same teleconnection (e.g., El Niño (year 0) and La Niña (year 0)) in a given month, and for similar phases in different months (e.g., El Niño (year 0) in March and October).

[35] Those spatial areas that are likely to experience substantially decreased mesocyclogenesis compared to climatology (i.e., −MCP) for SH teleconnection modes, also are determined. These are based on the overlap of mesocyclone-unfavorable conditions depicted on the reanalysis composites [cf. *Claud et al.*, 2009]. The unfavorable conditions generally are the opposite of those deemed favorable for mesocyclogenesis, as follows: positive anomalies of T500; negative SST-T925; northerly anomalies of **V**925; on-ice airflow. Because we emphasize the mesocyclogenesis potential (i.e., MCP) of teleconnections in this study, we determine only the lowest two probability categories of −MCP: "Not

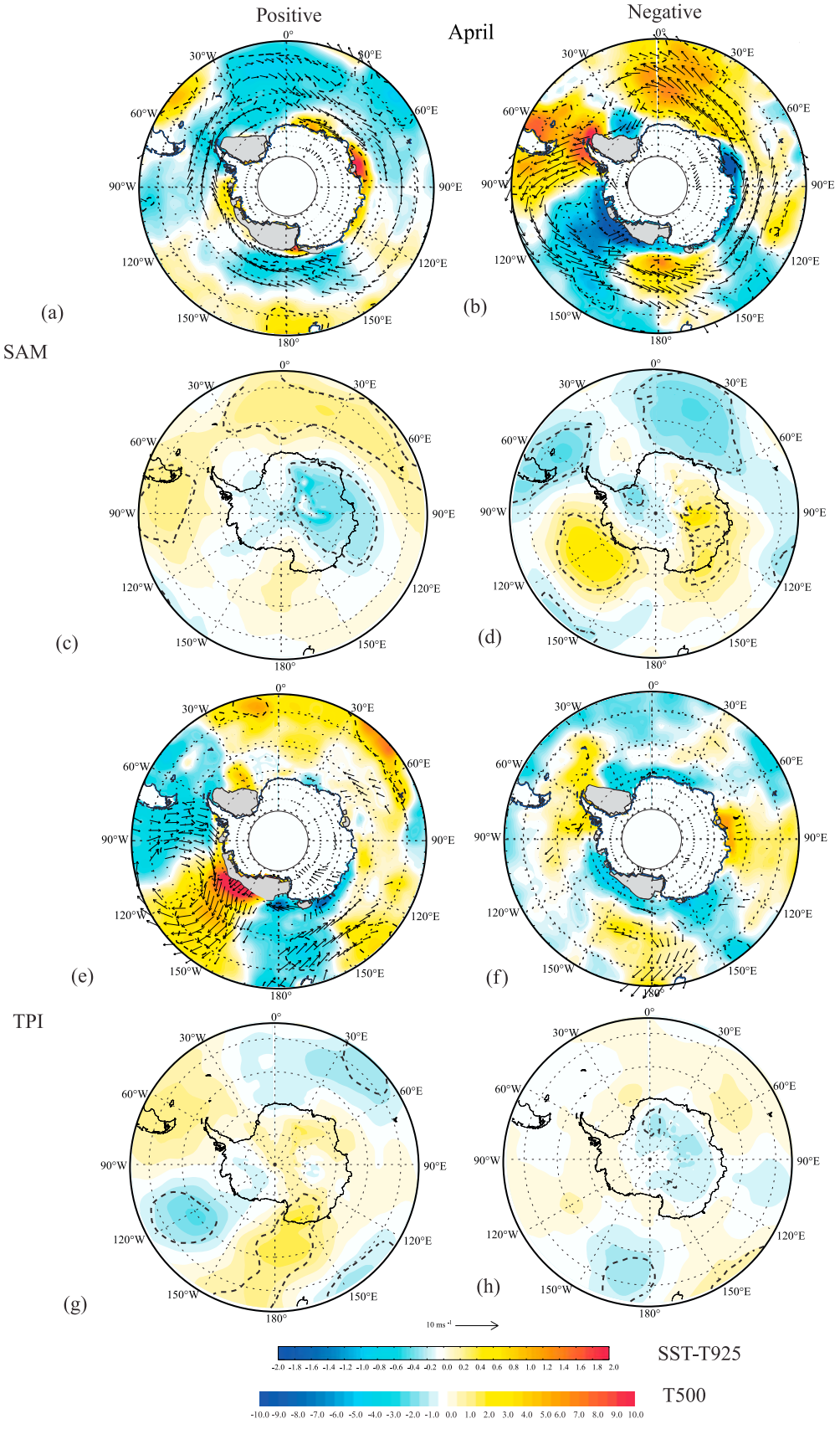

Figure 8. Similar to Figure 7 but for April and for (a–d) SAM and (e–g) TPI.

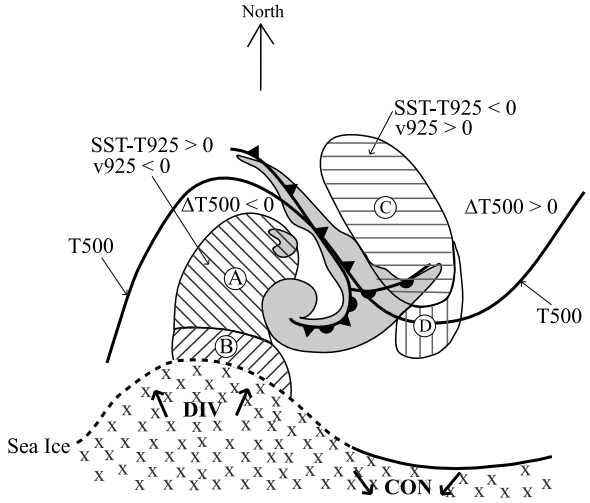

Figure 9. Spatial dependence of MCP categories High Probability (area A) and Maximum Probability (area B) and −MCP categories of Lowest Probability (area C) and Low Probability (area D), for coupled atmosphere and upper ocean anomalies in middle and higher southern latitudes associated with an anomalous trough-ridge pattern. The time-averaged "storm track" (oriented northwest to southeast) is denoted by the satellite-viewed frontal cloud vortex (the larger shaded signature); a smaller "Positive Vorticity Advection (PVA) maximum" (i.e., comma-cloud mesocyclone) is located just west of the frontal cyclone/storm track (both from *Guymer* [1978]). Divergence (convergence) of the pack ice and associated reduced (increased) ice concentration are shown by the dashed (solid) line demarcating the ice-ocean margin. The single line denoted T500 is a representative isotherm at the 500 hPa level and can also be considered a geopotential height contour at 500 hPa, owing to equivalent barotropy of the Southern Hemisphere extratropical atmosphere; a negative v925 (meridional component of **V**925) corresponds to a southerly wind. DIV, divergence; CON, convergence.

Favorable" (i.e., all but one unfavorable condition present); and "Least Favorable" (all mesocyclone-unfavorable conditions are present). These two low-probability categories represent the opposite of the MCP High and Maximum categories, respectively.

[36] The spatial dependencies of the two highest and two lowest probability classes of mesocyclogenesis potential (i.e., MCP, −MCP) are summarized schematically in Figure 9. These idealized relationships are shown with respect to the middle-to-higher-latitude storm track, represented by the typical satellite-viewed cloud vortex of a frontal cyclone [*Guymer*, 1978]; the associated midtropospheric geopotential height and thermal trough/ridge pattern (i.e., assuming equivalent barotropy [*van Loon and Kidson*, 1993]); the springtime sea ice extent and concentration; and Antarctic continental ice sheet margin (for early autumn associations). Accordingly, Figure 9 links the mesoscale patterns of mesocyclone-significant upper ocean and atmosphere variables depicted on the reanalysis composites (Figures 3–8) with the synoptic-scale atmospheric circulation; the latter varying by teleconnection phase. Higher MCP occurs in the cold-air advection west and southwest of the storm track, within the trough (i.e., negative T500), because this area typically has strongly positive SST-T925 and enhanced southerly anomalies of **V**925 [e.g., *Yuan et al.*, 1999]. Divergence in the lower level wind field west of the trough axis resulting from the Coriolis deflection [e.g., *Motoi et al.*, 1998; *Milliff et al.*, 1999] promotes upwelling of colder water on climatic time scales. The maximum values of MCP are located just equatorward of the sea-ice edge under off-ice airflow conditions because of the tendency for enhanced zonal gradients of SST and T925 to develop there [e.g., *Kottmeier and Hartig*, 1990]. These enhanced temperature gradients in the atmospheric boundary layer have been implicated in mesocyclogenesis events near the Antarctic sea ice edge [e.g., *Carleton and Fitch*, 1993]. In those longitudes (Figure 9), the sea ice is displaced equatorward of its mean position, with the maximum extent located just west of the thermal/geopotential trough axis. There, wind-induced ice divergence leads to reduced ice concentration, and appreciable ocean-to-atmosphere turbulent heat fluxes. In late summer and early autumn, when sea ice is absent from much of Antarctica, the MCP increases close to the continental ice sheet margin in areas of off-continent airflow (i.e., southerly winds): "column stretching" of air as it descends the ice sheet is believed to be important in the spin up of many such coastal mesocyclones [e.g., *Turner et al.*, 1993b; *Carrasco and Bromwich*, 1995; *Heinemann*, 1996].

[37] By contrast, east of the storm track, just west of the geopotential/thermal ridge axis, the probability of mesocyclogenesis is lowest (Figure 9): negative values of SST-T915 over which blow low-level northerly winds, tend to coincide with positive anomalies of T500. Moreover, the associated convergence in the lower level wind field promotes downwelling of ocean surface water [e.g., *Motoi et al.*, 1998; *Milliff et al.*, 1999]. In those longitudes also, the sea ice edge is located at higher latitudes as opposed to a location in and just west of the trough, and convergence of the pack increases the ice concentration. Accordingly, ocean-to-atmosphere fluxes of heat are reduced, and may even be reversed, especially under northerly airflow.

[38] The spatial patterns of MCP and −MCP are shown and discussed by teleconnection type and phase (Figures 10–13), for the start months of their respective transition seasons (i.e., October and March). The areas of lowest probability of mesocyclogenesis (i.e., −MCP) occupy unshaded areas on the MCP maps. The two sets of maps (MCP, −MCP) are not necessarily mirror images for a given teleconnection phase: areas of highest and lowest potential can be located in close proximity or some distance removed, depending on the composite reanalysis patterns and their statistical significance (section 4.2). As above, we discuss the patterns for October first, then March. We also comment upon the cross-seasonal persistence of the MCP patterns.

5.1. October

[39] Large differences in the reanalysis-indicated spatial patterns of MCP and −MCP between El Niño (year 0) and La Niña (year 0) events (Figures 10 and 11) are highly suggestive of a three-wave pattern. For El Niño (year 0), elevated MCP is "predicted" for ocean and adjacent sea-ice areas of the southern Indian Ocean, the southwest Pacific, and southwest Atlantic/Weddell Sea sector, with low

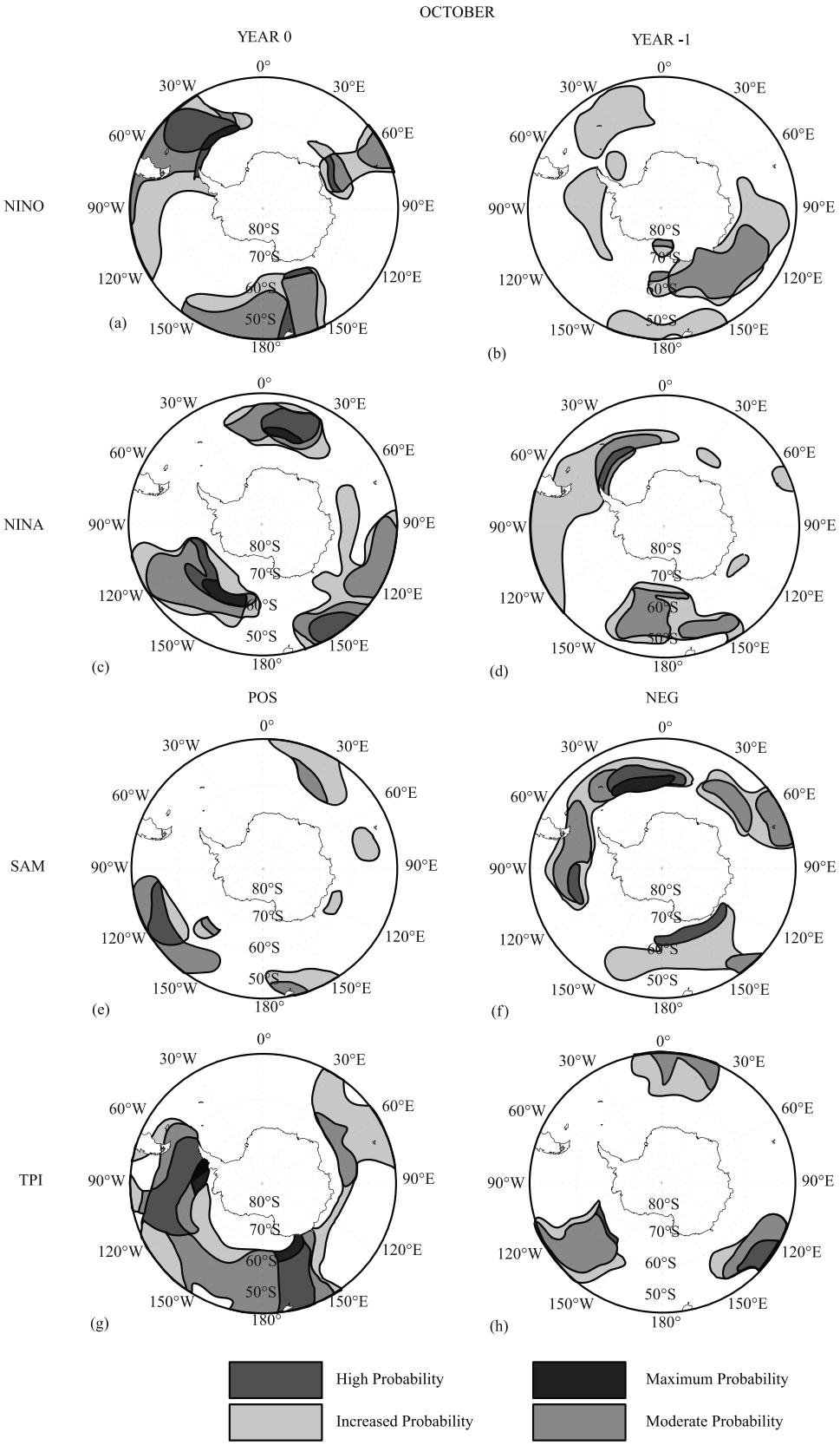

Figure 10. Maps of enhanced mesocyclogenesis (MCP) (refer to text) in October associated with large-scale teleconnections (four classes).

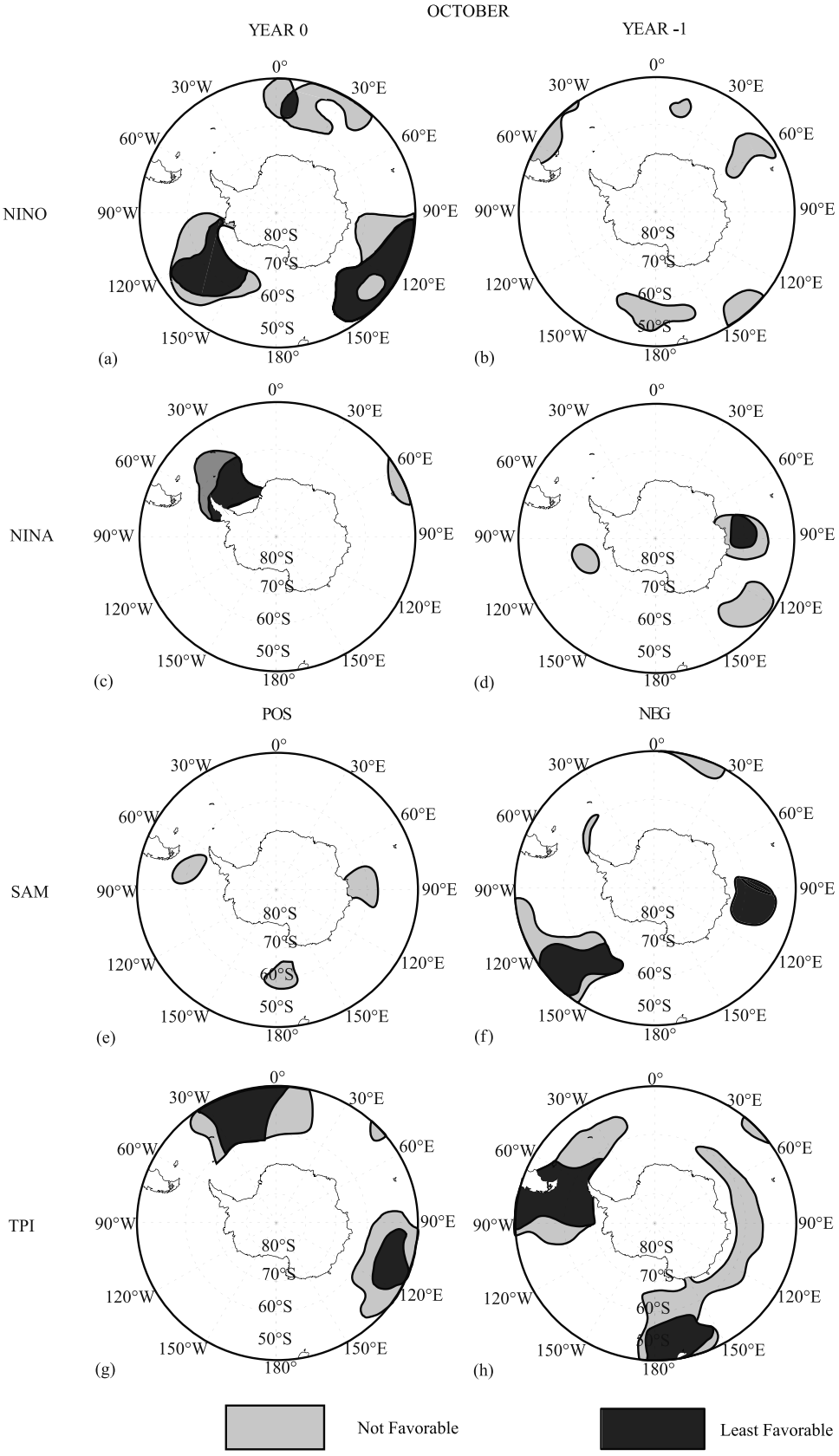

Figure 11. Maps of suppressed mesocyclogenesis potential, −MCP (refer to text), in October associated with large-scale teleconnections (two end probability classes).

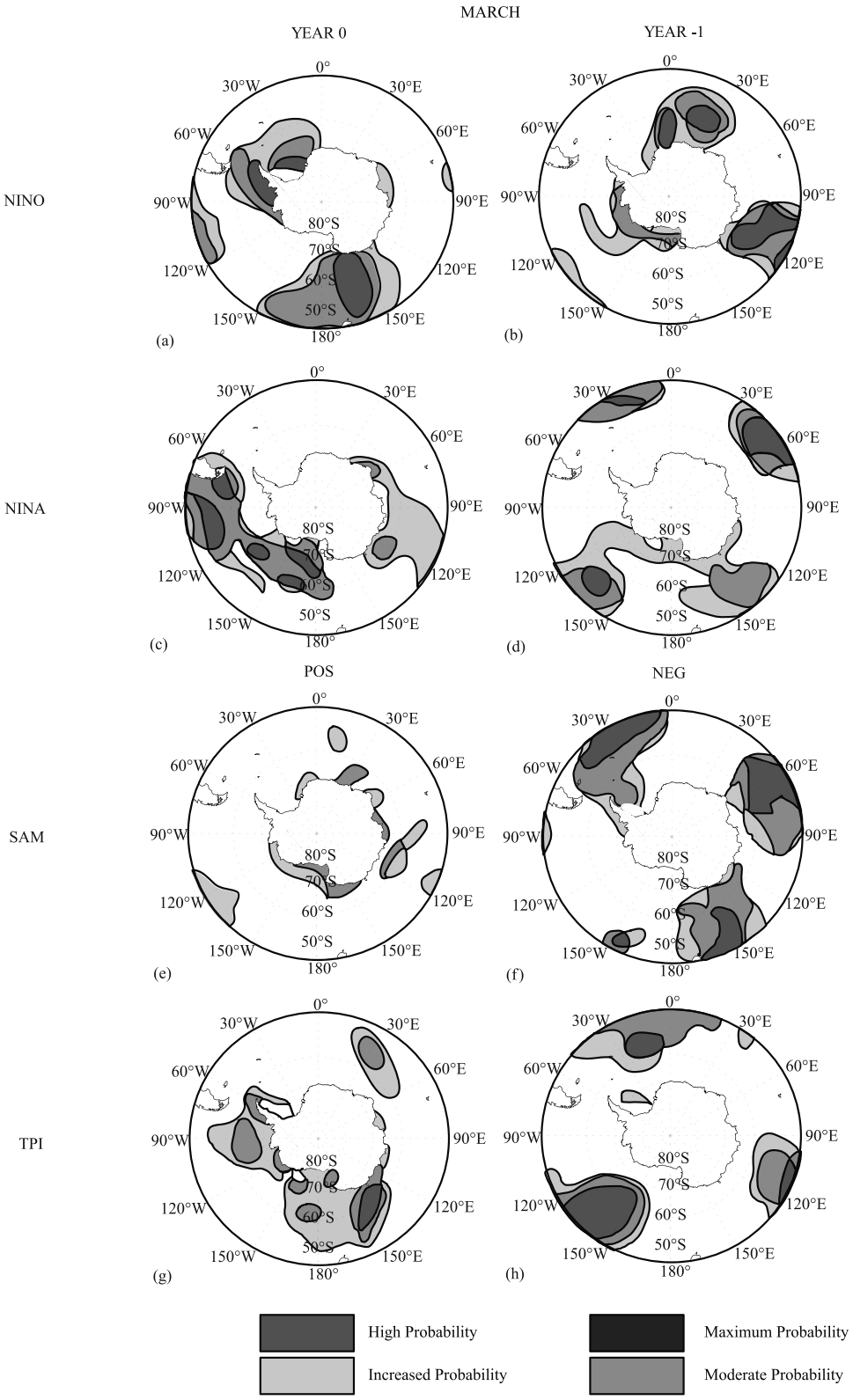

Figure 12. Similar to Figure 10 but for March.

probabilities (−MCP) in between. Those areas of low probability in El Niño (year 0) become the areas of strong MCP in La Niña (year 0) suggesting, as for the winter season [*Claud et al.*, 2009], that the intrahemispheric-scale variations of MCP are dominated by ENSO. Variations of MCP between ENSO phases (El Niño, La Niña) in year − 1 are not quite as large as those for year 0, although areal coverage of the High and Maximum probability categories increases particularly south of Australia in El Niño (year − 1). In La Niña (year − 1), relative to both El Niño (year − 1) and

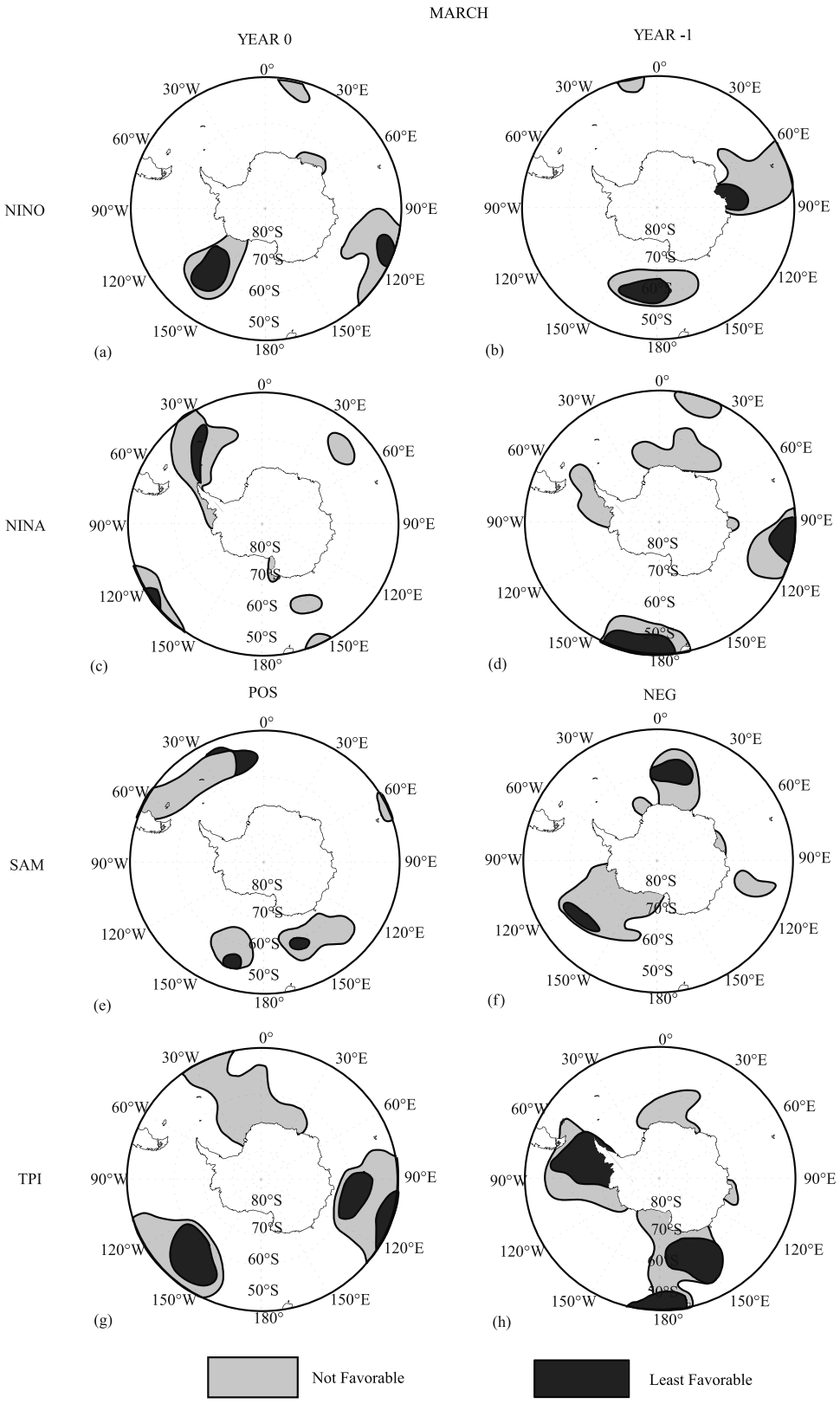

Figure 13. Similar to Figure 11 but for March.

La Niña (year 0), the biggest increases in MCP occur over middle to higher latitudes of the southwest Atlantic and south of New Zealand. Low probability of mesocyclogenesis (−MCP) in La Niña (year − 1) is suggested particularly near Antarctica at around 90°E, in contrast to La Niña (year 0), when a large area of −MCP is located in the Weddell Sea sector.

[40] The composite October months marked by negative SAM indicate a greater areal coverage of increased MCP compared to the corresponding months of positive SAM, especially over higher-middle latitudes (Figure 10). Interestingly, the area of strongly reduced mesocyclogenesis potential (−MCP) is also larger in October months having negative SAM than in the corresponding months of positive SAM (Figure 11). We compared our results for SAM with those obtained by *Lubin et al.* [2008] for the region covering the southeast Pacific through southwest Atlantic centered on the Antarctic Peninsula. For the period 1991–1994, these authors observed more mesocyclones just west of the Antarctic Peninsula under positive versus negative phases of the SAM, especially during winter, and to a lesser extent in spring. Our results differ, whereby we note an increase in mesocyclone formation potential from about 55°–62°S for negative SAM, and no clear association over higher latitudes. Reasons for these different results likely include the fact that *Lubin et al.* [2008] consider September to be a spring month, as well as a possible interference of their results with ENSO. We also note an increased potential for mesocyclone formation in October for El Niño year 0 just west of the Antarctic Peninsula.

[41] There is considerably greater areal coverage of MCP in composite October months marked by positive TPI than in corresponding months of negative TPI (Figure 10). While MCP for negative TPI suggests a three-wave pattern concentrated over middle latitudes, that for positive TPI increases generally for the South Pacific sector and also the southwest Indian Ocean. Areas of strongly decreased −MCP for positive TPI (Figure 11) occur in middle latitudes of the South Atlantic and southeast Indian Ocean, but these are located at somewhat higher latitudes in negative TPI; especially the Bellingshausen Sea through Drake Passage, and just south of New Zealand. Thus, the latitude zone of elevated MCP (decreased −MCP) tends to alternate between extreme phases of TPI: higher (middle) latitudes for positive TPI; middle (higher) latitudes for negative TPI.

5.2. March

[42] Similar to the patterns for October, in March there are large variations of MCP and −MCP between El Niño and La Niña (year 0), and also between the year 0 and year − 1 composites for the same phase of ENSO (Figures 12 and 13). For El Niño (year 0), broadly similar areas of the SH are predicted to see elevated MCP in composite March months as in October, with the exception of the Indian Ocean area which should see reduced activity. For El Niño (year − 1), the March composite shows greater differences from the corresponding October composite; notably, decreased activity in longitudes of New Zealand but strongly increased activity in the southeast Atlantic Ocean. Also similar to the October months, the March MCP for El Niño (year 0) and La Niña (year 0) shows more-or-less opposite geographic patterns: elevated activity for the Weddell Sea and south of New Zealand in El Niño (year 0), but greater MCP over the South Pacific Ocean in La Niña (year 0). For El Niño (year − 1), the MCP pattern similarly contrasts with that for El Niño (year 0): elevated MCP occurs in the areas that are predicted to have either near-average values of mesocyclogenesis potential or low probability (i.e., −MCP) in the following year. Generally the same can be said for La Niña (year − 1), although strong differences in MCP between year 0 and year − 1 for the South Pacific sector are restricted to longitudes eastward of about 120°W. Moreover, the area of −MCP extending from the eastern Bellingshausen Sea into the southwest Atlantic in La Niña (year 0) did not have elevated potential (MCP) the year before. Finally, it can be said that the MCP maps for El Niño (year − 1) and La Niña (year 0) show only limited similarity, mostly for the south central Pacific Ocean and southeast Indian Ocean [cf. *van Loon and Shea*, 1985; *Carleton*, 1988].

[43] The MCP for composite March months marked by extremes of the SAM, shows a contrasting pattern of elevated probability close to Antarctica (over middle and higher-latitude ocean areas) in the positive (negative) mode (Figure 12). The pattern of a larger area of strong MCP associated with negative SAM contrasted with positive SAM− and over broadly similar areas of the SH− was also evident for October (Figure 10). However, the pattern of elevated MCP adjacent to Antarctica for positive SAM was not evident in the corresponding MCP map for October, most likely because of the much greater extent of the sea ice in that month and its role in determining the MCP. The low-probability areas (−MCP) of each SAM mode occupy broadly the same latitude zone of the opposite mode's areas of elevated probability (MCP), similar to what was noted for TPI in October. In the work of *Lubin et al.* [2008], focusing on the mesocyclone activity in the region of the southeast Pacific through southwest Atlantic, there was no clear signal during autumn. In agreement with these authors, we also see no clear relationship of SAM with mesocyclogenesis in this region.

[44] For opposite modes of the TPI in March, strongly contrasting spatial patterns of MCP suggest a dominant meridional wave structure (Figure 12). In TPI positive phases, mesocyclogenesis is predicted to increase the most compared to background levels south of Australia and New Zealand, and also in the Amundsen/Bellingshausen seas and western Weddell Sea. Conversely, in negative TPI, elevated MCP is located in middle-to-higher latitudes of the South Pacific, the Atlantic, and the southeast Indian Ocean. Moreover, there is considerable similarity between the low-probability (i.e., −MCP) map of either TPI mode (Figure 13) with the high-probability (MCP) map of the opposite mode. This raises the possibility of a more-or-less linear relationship between TPI modes in terms of the associated mesocyclogenesis potential, that should be explored in future work.

5.3. Comparisons With Winter Season MCP

[45] We compare the October and March patterns with those derived for the winter season (specifically June) documented by *Claud et al.* [2009, Figures 14 and 15]. Although the October and March patterns are similar in terms of the area of the SH covered by elevated MCP (i.e., four classes of probability), for most teleconnection phases there is a greater area of the hemisphere involved in June. This is especially the case for La Niña (year 0 and year − 1), El Niño (year − 1), and Positive SAM. Because the average sea-ice area is greater in October than in June, this increased extent of MCP in the latter month likely results from the phase of the semiannual oscillation (SAO) and its role in determining the dominant latitude of the circumpolar trough and amount of cyclonic activity over the Southern Ocean.

The SAO has similar phase in March and October and an associated higher-latitude displacement of the circumpolar trough in those months, contrasted with June [e.g., *van Loon*, 1967; *van Loon and Rogers*, 1984]. Further, the correlation of ENSO and SAM over the period of interest (in both March and October, 0.56 and −0.57, respectively), and the fact that SAM has been mostly positive during 1979–2001, likely contribute to this result through preventing us from fully disentangling the effect of each teleconnection.

[46] To gain insights into the temporal persistence of the spatial patterns, we intercompare MCP maps by teleconnection type and phase for March, June, and October. For ENSO, the MCP map for June (year 0) should be compared with that of March (year − 1), rather than the March (year 0) map, because it is for 3 months earlier as opposed to 9 months later. Specifically, for El Niño, areas of elevated MCP occur over the South Atlantic and southeast Indian Ocean in both June (year 0) and March (year − 1), with the latter month also showing increased potential at high latitudes in the Ross Sea and eastward to the Antarctic Peninsula. This is likely a result of the lack of sea ice in the early autumn. Similarly for La Niña, elevated MCP occupies the three ocean basins in both June (year 0) and March (year − 1), although these areas are larger in June, as noted above.

[47] The MCP maps for June and October pertain to year 0 (i.e., they are 4 months apart), and so may reasonably be compared by teleconnection type and phase. Subjective comparisons of MCP spatial patterns in June and October for ENSO suggest somewhat less similarity than between March (year − 1) and June, especially for El Niño. Again, these differences may result from the different SAO phase and its influence on the latitude of the circumpolar trough, in combination with the near-maximum extent of sea ice in October. A similarly reduced persistence in the spatial patterns of MCP between June and October is evident for SAM positive and negative phases. However, the spatial consistency of MCP in June and October appears considerably higher for TPI, especially the negative phase. The absence of a significant correlation between TPI and the two other teleconnections (Table 3) may help explain this higher spatial consistency, contrasted with those of ENSO and SAM.

[48] Regionally, and in a given year, marked month-to-month variations of mesocyclone activity can occur (e.g., the region south of Australia in October and November 1992, CS97). However, the above composite results raise the issue of the representative nature of the transition season start month (October, March) and its ability to depict MCP patterns of its respective season (spring, autumn). Examining MCP patterns by teleconnection mode and phase for November and April (not shown), indicates general similarity with the preceding month (October, March) in terms of spatial pattern, although there are differences of detail. These characteristics likely result from the stronger spatial persistence of T500 anomalies between consecutive months, contrasted with SST-T925 or **V**925.

5.4. Potential Mechanisms

[49] Although climatic simulations would be necessary to fully assess the mechanisms underlying the features observed in the MCP maps, a few remarks can nevertheless be made, as follows.

[50] 1. For ENSO, Niño years are associated with a storm track shifted equatorward in the South Pacific but poleward in the Atlantic [*Rind et al.*, 2001]. This pattern is accompanied by a high (low) pressure anomaly over the Bellingshausen (Weddell) seas, and corresponding regional circulations that bring warm air to high latitudes of the Pacific and cold air out of the Antarctic continent over the southwest Atlantic [*Carleton*, 1988; *Yuan and Martinson*, 2001]. These combined effects explain the reduced frequencies of mesocyclones over the Bellingshausen and Amundsen seas, and the increased frequencies over the Weddell Sea for Niño years (and the opposite for Niña years).

[51] 2. For SAM, a positive phase implies a poleward shift of the storm track; because many mesocyclones develop in cold air behind frontal cyclones, one would expect more mesocyclones over higher latitudes. Indeed, this is observed in March with more mesocyclones around the Antarctic coast, but not in October, when the sea ice extent is much greater. However, in October, mesocyclone frequencies increase for the SAM negative phase at around 55°S because of the equatorward shift of the storm track. The area between 100° and 150°W generally displays opposite features to the other longitudes, probably in association with the nonannular SST response to SAM [e.g., *Lovenduski and Gruber*, 2005].

[52] 3. The association of MCP with TPI is linked to the intensity and location of the trough and ridge that express the variations in wave number one, and the fact that mesocyclones form preferentially to the west of troughs and east of ridges, owing to the combined southerly wind anomalies, cold-air advection, upward convective heat fluxes and likely also, strong equatorward advances in the sea ice edge. Thus, the storm track and associated polar-front jet stream are displaced equatorward (poleward) in longitudes of the troughs (ridges).

[53] These observations suggest that the displacement of the storm track plays a major role in the associations between mesocyclones and teleconnections; an additional ingredient is the position of the sea ice border relative to the storm track.

6. Summary

[54] In this study, the climatic environments of SH cold-air mesocyclones and their associations with teleconnections were investigated for transition season months. Several reasons motivated such a study, as follows: (1) The relatively few studies undertaken for the transition season months suggested that they have the highest frequencies of mesocyclones, possibly the result of the semiannual oscillation that dominates over sub-Antarctic latitudes and which reaches its maxima in the spring and autumn seasons. (2) A clear ENSO response was expected because its climatic ''signal'' over middle and higher southern latitudes strengthens (weakens), on average, in austral springtime (autumn), thereby providing another point of comparison with the mesocyclone activity. (3) The Antarctic sea-ice conditions typically change rapidly during the spring and autumn, and the ice is near its maximum (minimum) extent, on average, in October (March). The ultimate objective of our study is to improve climatic (i.e., seasonal/subseasonal)

predictions of cold-air mesocyclogenesis over the Southern Ocean during these months.

[55] We identified the associated composite atmospheric and upper oceanic large-scale environments of mesocyclones on monthly time scales. This first step relied on the use of both the long-term high-resolution daily ERA-40 reanalysis and inventories of cold-air mesocyclones based on satellite image interpretation for case-study months of March–April and October–November in 1988 and 1992. Although these inventories were restricted to portions of the SH, we showed that mesocyclones occur preferentially in association with either low temperatures at 500 hPa or proximity to large gradients of T500. Additional favorable conditions for mesocyclones include a large positive difference in SST-T925, coincident with south to southwesterly low-level winds (**V**925) (i.e., implying strong upward fluxes of heat and moisture occurring to the west and southwest of midtropospheric troughs and frontal cyclones). An additional mesocyclone-favorable condition in the spring months is proximity to the sea ice. Conversely, unfavorable conditions for mesocyclogenesis include warm air at 500 hPa; negative or only weakly positive SST-T925; northerly low-level winds that blow over these cool waters (i.e., stable lower atmosphere); and reduced sea ice extent relative to normal (i.e., implying downward fluxes of heat east of frontal cyclones and west of high-pressure ridges). It should also be noted that important local factors in mesocyclogenesis, such as katabatic winds, are not explicitly considered here although their influence can be manifest in variables such as greater local sea ice extent and more strongly positive SST-T925 values offshore. Such an assessment would require specific investigations at smaller scales that are difficult to achieve with the present spatial resolution of the reanalyses and the available satellite-based mesocyclone inventories.

[56] The second objective of the study was to determine spatial associations of reanalysis variables favorable to mesocyclogenesis according to the three large-scale SH teleconnection patterns (ENSO, SAM, TPI). All variables show an association with the three teleconnections, although these are generally weaker than for the winter months: standardized anomalies are of smaller amplitude, the 90% significance level generally covers smaller regions, and the variables seldom behave congruently. Possibly contributing to this last point is that, contrary to the winter months, the teleconnection indices for some transition season months are significantly intercorrelated. Notwithstanding, we observed that in spring, the intrahemispheric variability of mesocyclogenesis is dominated by ENSO. The SAM and TPI remain influential, with the latter teleconnection suggesting a three-wave pattern within the latitude zone under consideration. This results in more (fewer) mesocyclones over higher (middle) latitudes for positive TPI, and more (fewer) mesocyclones for middle (higher) latitudes for negative TPI. In autumn, ENSO, SAM, and TPI are about equally influential but their response varies regionally. As for spring, large variations between El Niño and La Niña are noted. A positive SAM tends to enhance mesocyclogenesis in regions adjacent to Antarctica, while a dominant meridional wave structure is suggested for TPI. In addition, consideration of the phase of the SAO and its influence on the latitude zone of maximum cyclonic activity over the Southern Ocean is essential to the interpretation of the results. Modeling work is needed to clearly identify the mechanisms governing these associations, but our results suggest that the displacement of the storm track between opposite phases of a given teleconnection appears to play a major role.

[57] Our results are also relevant to the role of teleconnections in a changing climate; in particular, the positive SAM trend may continue longer term [*Bracegirdle et al.*, 2008], the SAO temporal trend [*van den Broeke*, 1998] may either continue or reverse as a result of the strong warming of West Antarctica [*Steig et al.*, 2009], and the recent warming noted for East Antarctica could become statistically significant in the near future. High-latitude climate changes such as these almost inevitably will affect the frequencies, and possibly also key longitudes, of cold-air outbreaks and their associated mesocyclone activity (cf. *Kolstad and Bracegirdle* [2008] for the Arctic). In turn, these cross-scale atmospheric associations will likely alter the development of Antarctic coastal polynyi and, accordingly, the formation of Antarctic bottom water, resulting in longer-term climate changes.

[58] Finally, this study points to the need for long-term hemisphere-wide satellite-based mesocyclone climatologies developed explicitly for transition season months, thereby spanning a range of teleconnection phases, and against which the MCP and −MCP maps may be corroborated.

[59] **Acknowledgments.** The support of U.S. National Science Foundation grants SES-8603470, DPP-8816912, and OPP-9219446 to Andrew M. Carleton is gratefully acknowledged. We are grateful to the three anonymous reviewers, whose insightful comments benefited the final paper. The ERA-40 data were obtained from the ECMWF Data Server. S. Masson provided graphical software (SAXO) for plotting the results.

References

Blechschmidt, A. M. (2008), A 2-year climatology of polar low events over the Nordic Seas from satellite remote sensing, *Geophys. Res. Lett.*, *35*, L09815, doi:10.1029/2008GL033706.

Bracegirdle, T. J., and S. L. Gray (2008), An objective climatology of the dynamical forcing of polar lows in the Nordic Seas, *Int. J. Climatol.*, *28*, 1903–1919, doi:10.1002/joc.1686.

Bracegirdle, T. J., W. M. Connolley, and J. Turner (2008), Antarctic climate change over the twenty first century, *J. Geophys. Res.*, *113*, D03103, doi:10.1029/2007JD008933.

Bromwich, D. H. (1991), Mesoscale cyclogenesis over the south-western Ross Sea linked to strong katabatic winds, *Mon. Weather Rev.*, *119*, 1736–1752, doi:10.1175/1520-0493(1991)119<1736:MCOTSR>2.0.CO;2.

Bromwich, D. H., and R. T. Fogt (2004), Strong trends in the skill of the ERA-40 and NCEP-NCAR reanalyses in the high and middle latitudes of the Southern Hemisphere, 1958–2001, *J. Clim.*, *17*, 4603–4619, doi:10.1175/3241.1.

Bromwich, D. H., A. N. Rogers, P. Kållberg, R. I. Cullather, J. W. C. White, and K. J. Kreutz (2000), ECMWF analyses and reanalyses depiction of ENSO signal in Antarctic precipitation, *J. Clim.*, *13*, 1406–1420, doi:10.1175/1520-0442(2000)013<1406:EAARDO>2.0.CO;2.

Businger, S. (1985), The synoptic climatology of polar-low outbreaks, *Tellus, Ser. A*, *37*, 419–432.

Businger, S. (1987), The synoptic climatology of polar-low outbreaks over the Gulf of Alaska and the Bering Sea, *Tellus, Ser. A*, *39*, 307–325.

Businger, S., and R. J. Reed (1989), Cyclogenesis in cold air masses, *Weather Forecasting*, *4*, 133–156, doi:10.1175/1520-0434(1989)004<0133:CICAM>2.0.CO;2.

Carleton, A. M. (1979), A synoptic climatology of satellite-observed extratropical cyclone activity for the Southern Hemisphere winter, *Theor. Appl. Climatol.*, *27*, 265–279, doi:10.1007/BF02246649.

Carleton, A. M. (1987), Satellite-derived attributes of cloud vortex systems and their application to climate studies, *Remote Sens. Environ.*, *16*, 2457–2485.

Carleton, A. M. (1988), Sea ice–atmosphere signal of the Southern Oscillation in the Weddell Sea, Antarctica, *J. Clim.*, *1*, 379–388, doi:10.1175/1520-0442(1988)001<0379:SISOTS>2.0.CO;2.

Carleton, A. M. (1989), Antarctic sea-ice relationships with indices of the atmospheric circulation of the Southern Hemisphere, *Clim. Dyn.*, *3*, 207–220, doi:10.1007/BF01058236.

Carleton, A. M. (1992), Synoptic interactions between Antarctica and lower latitudes, *Aust. Meteorol. Mag.*, *40*, 129–147.

Carleton, A. M. (1995), On the interpretation and classification of mesoscale cyclones from satellite infrared imagery, *Int. J. Remote Sens.*, *16*, 2457–2485, doi:10.1080/01431169508954569.

Carleton, A. M. (2003), Atmospheric teleconnections involving the Southern Ocean, *J. Geophys. Res.*, *108*(C4), 8080, doi:10.1029/2000JC000379.

Carleton, A. M., and D. A. Carpenter (1989), Intermediate-scale sea ice–atmosphere interactions over high southern latitudes in winter, *GeoJournal*, *18*, 87–101, doi:10.1007/BF00722392.

Carleton, A. M., and D. Carpenter (1990), Satellite climatology of "polar lows" and broadscale climatic associations for the Southern Hemisphere, *Int. J. Climatol.*, *10*, 219–246, doi:10.1002/joc.3370100302.

Carleton, A. M., and M. Fitch (1993), Synoptic aspects of Antarctic mesocyclones, *J. Geophys. Res.*, *98*, 12,997–13,018, doi:10.1029/92JD02132.

Carleton, A. M., and Y. Song (1997), Synoptic climatology and intrahemispheric associations of cold air mesocyclones in the Australasian sector, *J. Geophys. Res.*, *102*, 13,873–13,887, doi:10.1029/96JD03357.

Carleton, A. M., and Y. Song (2000), Satellite passive sensing of the marine atmosphere associated with cold-air mesoscale cyclones, *Prof. Geogr.*, *52*, 289–306, doi:10.1111/0033-0124.00225.

Carrasco, J. F., and D. H. Bromwich (1994), A survey of mesoscale cyclonic activity near McMurdo Station, Antarctica, *Antarct. J. U. S.*, *29*, 298–301.

Carrasco, J. F., and D. H. Bromwich (1995), A case study of a midtropospheric subsynoptic-scale cyclone that developed over the Ross Sea and Ross Ice Shelf of Antarctica, *Antarct. Sci.*, *7*, 199–210, doi:10.1017/S0954102095000277.

Carrasco, J. F., and D. H. Bromwich (1996), Mesoscale cyclone activity near Terra Nova Bay and Byrd Glacier, Antarctica during 1991, *Global Atmos. Ocean Syst.*, *5*, 43–72.

Carrasco, J. F., D. H. Bromwich, and Z. Liu (1997a), Mesoscale cyclone activity over Antarctica during 1991: 1. Mary Bird Land, *J. Geophys. Res.*, *102*, 13,923–13,937, doi:10.1029/97JD00905.

Carrasco, J. F., D. H. Bromwich, and Z. Liu (1997b), Mesoscale cyclone activity over Antarctica during 1991: 2. Near the Antarctic Peninsula, *J. Geophys. Res.*, *102*, 13,939–13,954, doi:10.1029/97JD00904.

Carrasco, J. F., D. H. Bromwich, and A. J. Monaghan (2003), Distribution and characteristics of mesoscale cyclones in the Antarctic: Ross Sea eastward to the Weddell Sea, *Mon. Weather Rev.*, *131*, 289–301, doi:10.1175/1520-0493(2003)131<0289:DACOMC>2.0.CO;2.

Cavalieri, D., C. Parkinson, P. Gloersen, and H. J. Zwally (1996), Sea ice concentrations from Nimbus-7 SMMR and DMSP SSM/I passive microwave data, http://nsidc.org/data/seaice_index, Natl. Snow and Ice Data Cent., Boulder, Colo. (Updated 2006.)

Claud, C., K. B. Katsaros, G. W. Petty, A. Chedin, and N. A. Scott (1992a), A cold air outbreak over the Norwegian Sea observed with the TIROS-N Operational Vertical Sounder (TOVS) and the Special Sensor Microwave Imager (SSM/I), *Tellus, Ser. A*, *44*, 100–118.

Claud, C., N. A. Scott, and A. Chedin (1992b), Use of TOVS observations for the study of polar and arctic lows, *Int. J. Remote Sens.*, *13*, 129–139, doi:10.1080/01431169208904030.

Claud, C., N. M. Mognard, K. B. Katsaros, A. Chedin, and N. A. Scott (1993), Satellite observations of a polar low over the Norwegian Sea by Special Sensor Microwave/Imager, Geosat and TIROS-N Operational Vertical Sounder, *J. Geophys. Res.*, *98*, 14,487–14,506, doi:10.1029/93JC00650.

Claud, C., G. Heinemann, E. Raustein, and L. McMurdie (2004), Polar low *le Cygne*: Satellite observations and numerical simulations, *Q. J. R. Meteorol. Soc.*, *130*, 1075–1102, doi:10.1256/qj.03.72.

Claud, C., B. Duchiron, and P. Terray (2007), Associations between large-scale atmospheric circulation and polar low developments over the North Atlantic during winter, *J. Geophys. Res.*, *112*, D12101, doi:10.1029/2006JD008251.

Claud, C., A. M. Carleton, B. Duchiron, and P. Terray (2009), Southern Hemisphere winter cold-air mesocyclones: Climatic environments and associations with teleconnections, *Clim. Dyn.*, *33*, 383–408, doi:10.1007/s00382-008-0468-5.

Condron, A., G. R. Bigg, and I. Renfrew (2006), Polar mesoscale cyclones in the northeast Atlantic: Comparing climatologies from ERA-40 and satellite imagery, *Mon. Weather Rev.*, *134*(5), 1518–1533.

Condron, A., G. R. Bigg, and I. A. Renfrew (2008), Modeling the impact of polar mesocyclones on ocean circulation, *J. Geophys. Res.*, *113*, C10005, doi:10.1029/2007JC004599.

Cullather, R. I., D. H. Bromwich, and M. L. van Woert (1996), Interannual variations in Antarctic precipitation related to El Niño Southern Oscillation, *J. Geophys. Res.*, *101*, 19,109–19,118, doi:10.1029/96JD01769.

Davison, A. C., and D. V. Hinkley (1997), *Bootstrap Methods and Their Application*, 582 pp., Cambridge Univ. Press, New York.

Duncan, C. N. (1977), A numerical investigation of polar lows, *Q. J. R. Meteorol. Soc.*, *103*, 255–267, doi:10.1002/qj.49710343604.

Emanuel, K. A. (1986), An air-sea interaction theory for tropical cyclones. Part I: Steady-state maintenance, *J. Atmos. Sci.*, *43*, 585–604, doi:10.1175/1520-0469(1986)043<0585:AASITF>2.0.CO;2.

Emanuel, K. A., and R. Rotunno (1989), Polar lows as arctic hurricanes, *Tellus, Ser. A*, *41*, 1–17.

Ese, T., I. Kanestrom, and K. Pedersen (1988), Climatology of polar lows over the Norwegian and Barents seas, *Tellus, Ser. A.*, *40*, 248–255.

Fitch, M., and A. M. Carleton (1992), Antarctic mesocyclone regimes from satellite and conventional data, *Tellus, Ser. A*, *44*, 180–196.

Fogt, R. L., and D. H. Bromwich (2006), Decadal variability of the ENSO teleconnection to the high latitude South Pacific governed by coupling with the Southern Annular Mode, *J. Clim.*, *19*, 979–997, doi:10.1175/JCLI3671.1.

Forbes, G. S., and W. D. Lottes (1985), Classification of mesoscale vortices in polar airstreams and the influence of the large-scale environment on their evolution, *Tellus, Ser. A*, *37*, 132–155.

Gong, D., and S. Wang (1999), Definition of Antarctic oscillation index, *Geophys. Res. Lett.*, *26*, 459–462, doi:10.1029/1999GL900003.

Guymer, L. B. (1978), Operational application of satellite imagery to synoptic analysis in the Southern Hemisphere, *Tech. Rep. 29*, 87 pp., Dep. of Sci., Commonw. Bur. of Meteorol., Melbourne, Victoria, Australia.

Harangozo, S. A. (1997), Atmospheric meridional circulation impacts on contrasting winter sea ice extent in two years in the Pacific sector of the Southern Ocean, *Tellus, Ser. A*, *49*, 388–400, doi:10.1034/j.1600-0870.1997.t01-2-00006.x.

Harold, J. M., G. R. Bigg, and J. Turner (1999), Mesocyclone activity over the Northeast Atlantic. Part 2: Vortex distribution and variability, *Int. J. Climatol.*, *19*, 1283–1299, doi:10.1002/ (SICI)1097-0088(199910)19:12<1283::AID-JOC420>3.0.CO;2-T.

Harrold, T. W., and K. A. Browning (1969), The polar low as a baroclinic disturbance, *Q. J. R. Meteorol. Soc.*, *95*, 710–723, doi:10.1002/qj.49709540605.

Heinemann, G. (1990), Mesoscale vortices in the Weddell Sea region (Antarctica), *Mon. Weather Rev.*, *118*, 779–793, doi:10.1175/1520-0493(1990)118<0779:MVITWS>2.0.CO;2.

Heinemann, G. (1996), Three-dimensional structures of summertime Antarctic meso-scale cyclones: Part I: Observational studies with aircraft, satellite and conventional data, *Global Atmos. Ocean Syst.*, *4*, 149–180.

Heinemann, G., and C. Claud (1997), Report of a workshop on "Theoretical and observational studies of polar lows" of the European Geophysical Society Polar Lows Working Group, *Bull. Am. Meteorol. Soc.*, *78*, 2643–2658.

Hewson, T. D., G. C. Craig, and C. Claud (2000), Evolution and mesoscale structure of a polar low outbreak, *Q. J. R. Meteorol. Soc.*, *126*, 1031–1063, doi:10.1256/smsqj.56410.

Karoly, D. J. (1990), The role of transient eddies in low-frequency zonal variations of the Southern Hemisphere circulation, *Tellus, Ser. A*, *42*, 41–50.

Kidson, J. W. (1999), Principal modes of Southern Hemisphere low-frequency variability obtained from NCEP-NCAR reanalyses, *J. Clim.*, *12*, 2808–2830, doi:10.1175/1520-0442(1999)012<2808:PMOSHL>2.0.CO;2.

Kolstad, E. W., and T. J. Bracegirdle (2008), Marine cold-air outbreaks in the future: An assessment of IPCC AR4 model results for the Northern Hemisphere, *Clim. Dyn.*, *30*, 871–885, doi:10.1007/s00382-007-0331-0.

Kottmeier, C., and R. Hartig (1990), Winter observations of the atmosphere over Antarctic sea ice, *J. Geophys. Res.*, *95*, 16,551–16,560, doi:10.1029/JD095iD10p16551.

L'Heureux, M., and D. W. J. Thompson (2006), Observed relationships between the El Niño–Southern Oscillation and the extratropical zonal-mean circulation, *J. Clim.*, *19*, 276–287, doi:10.1175/JCLI3617.1.

Limpasuvan, V., and D. H. Hartmann (1999), Eddies and the annular modes of climate variability, *Geophys. Res. Lett.*, *26*, 3133–3136, doi:10.1029/1999GL010478.

Limpasuvan, V., and D. H. Hartmann (2000), Wave-maintained annular modes of climate variability, *J. Clim.*, *13*, 4414–4429, doi:10.1175/1520-0442(2000)013<4414:WMAMOC>2.0.CO;2.

Lovenduski, N. S., and N. Gruber (2005), Impact of the Southern Annular Mode on Southern Ocean circulation and biology, *Geophys. Res. Lett.*, *32*, L11603, doi:10.1029/2005GL022727.

Lubin, D., R. A. Wittenmyer, D. H. Bromwich, and G. J. Marshall (2008), Antarctic Peninsula mesoscale cyclone variability and climatic impacts influenced by the SAM, *Geophys. Res. Lett.*, *35*, L02808, doi:10.1029/2007GL032170.

Lyons, S. W. (1983), Characteristics of intense Antarctic depressions near the Drake Passage, in *Preprint Volume: First International Conference on Southern Hemisphere Meteorology, San Jose dos Campos, Brazil, July 31–August 6, 1983*, pp. 238–240, Am. Meteorol. Soc., Boston, Mass.

Mansfield, D. A. (1974), Polar lows: The development of baroclinic disturbances in cold air outbreaks, *Q. J. R. Meteorol. Soc.*, *100*, 541–554, doi:10.1002/qj.49710042604.

Marshall, G. J. (2003), Trends in the southern annular mode from observations and reanalyses, *J. Clim.*, *16*, 4134–4143, doi:10.1175/1520-0442(2003)016<4134:TITSAM>2.0.CO;2.

McMurdie, L. A., C. Claud, and S. Atakturk (1997), Satellite-derived characteristics of spiral and comma-shaped southern hemisphere mesocyclones, *J. Geophys. Res.*, *102*, 13,889–13,905, doi:10.1029/97JD00279.

Milliff, R. F., T. J. Hoar, H. van Loon, and M. Raphael (1999), Quasi-stationary wave variability in NSCAT winds, *J. Geophys. Res.*, *104*, 11,425–11,435, doi:10.1029/1998JC900087.

Motoi, T., A. Kitoh, and H. Koide (1998), Antarctic Circumpolar Wave in a coupled ocean-atmosphere model, *Ann. Glaciol.*, *27*, 483–487.

Nordeng, T. E., and E. A. Rasmussen (1992), A most beautiful polar low: A case study of a polar low development in the Bear Island region, *Tellus, Ser. A*, *44*, 81–99.

Pittock, A. B. (1980), Patterns of climatic variations in Argentina and Chile - 1. Precipitation, 1931–60, *Mon. Weather Rev.*, *108*, 1347–1361, doi:10.1175/1520-0493(1980)108<1347:POCVIA>2.0.CO;2.

Pittock, A. B. (1984), On the reality, stability and usefulness of Southern Hemisphere teleconnections, *Aust. Meteorol. Mag.*, *32*, 75–82.

Rasmussen, E. A. (1979), The polar low as an extratropical CISK disturbance, *Q. J. R. Meteorol. Soc.*, *105*, 531–549, doi:10.1002/qj.49710544504.

Rasmussen, E. A. (1981), An investigation of a polar low with a spiral cloud structure, *J. Atmos. Sci.*, *38*, 1785–1792, doi:10.1175/1520-0469(1981)038<1785:AIOAPL>2.0.CO;2.

Rasmussen, E. A. (1989), A comparative study of tropical cyclones and polar lows, in *Polar and Arctic Lows*, edited by P. F. Twitchell, E. A. Rasmussen, and K. L. Davidson, pp. 47–80, A. Deepak, Hampton, Va.

Rasmussen, E. A., and J. Turner (2003), *Polar Lows: Mesoscale Weather Systems in the Polar Regions*, 612 pp., Cambridge Univ. Press, New York.

Rasmussen, E. A., T. S. Pedersen, L. T. Pedersen, and J. Turner (1992), Polar lows and arctic instability lows in the Bear Island region, *Tellus, Ser. A*, *44*, 133–154.

Reed, R. J. (1979), Cyclogenesis in polar airstreams, *Mon. Weather Rev.*, *107*, 38–52, doi:10.1175/1520-0493(1979)107<0038:CIPAS>2.0.CO;2.

Renwick, J. A. (2004), Trends in the Southern Hemisphere polar vortex in NCEP and ECMWF reanalyses, *Geophys. Res. Lett.*, *31*, L07209, doi:10.1029/2003GL019302.

Rind, D., M. Chandler, J. Lerner, D. G. Martinson, and X. Yuan (2001), The climate response to basin-specific changes in latitudinal temperature gradients and the implications for sea ice variability, *J. Geophys. Res.*, *106*, 20,161–20,173, doi:10.1029/2000JD900643.

Rogers, J. C., and H. van Loon (1982), Spatial variability of sea level pressure and 500 mb height anomalies over the Southern Hemisphere, *Mon. Weather Rev.*, *110*, 1375–1392, doi:10.1175/1520-0493(1982)110<1375:SVOSLP>2.0.CO;2.

Simmons, A. J., and J. K. Gibson (2000), *The ERA-40 Project Plan, ERA-40 Proj. Rep. Ser., 2000*, vol. 1, 63 pp., Eur. Cent. for Medium-Range Weather Forecasts, Reading, U. K.

Sinclair, M. R., and X. Cong (1992), Polar air stream cyclogenesis in the Australasian region: A composite study using ECMWF analyses, *Mon. Weather Rev.*, *120*, 1950–1972, doi:10.1175/1520-0493(1992)120<1950:PACITA>2.0.CO;2.

Smith, T. S., and R. W. Reynolds (2003), Extended reconstruction of global sea surface temperatures based on COADS data (1854–1997), *J. Clim.*, *16*, 1495–1510, doi:10.1175/1520-0442(2003)016<1495:EROGSS>2.0.CO;2.

Smith, T. S., and R. W. Reynolds (2004), Improved extended reconstruction of SST (1854–1997), *J. Clim.*, *17*, 2466–2477, doi:10.1175/1520-0442(2004)017<2466:IEROS>2.0.CO;2.

Steig, E. J., D. P. Schneider, S. D. Rutherford, M. E. Mann, J. C. Comiso, and D. T. Shindell (2009), Warming of the Antarctic ice-sheet surface since the 1957 International Geophysical Year, *Nature*, *457*, 459–462, doi:10.1038/nature07669.

Sterl, A. (2004), On the (in)homogeneity of reanalysis products, *J. Clim.*, *17*, 3866–3873, doi:10.1175/1520-0442(2004)017<3866:OTIORP>2.0.CO;2.

Streten, N. A., and A. J. Troup (1973), A synoptic climatology of satellite-observed cloud vortices over the Southern Hemisphere, *Q. J. R. Meteorol. Soc.*, *99*, 56–72, doi:10.1002/qj.49709941906.

Thomas, E. R., G. J. Marshall, and J. R. McConnell (2008), A doubling in snow accumulation in the western Antarctic Peninsula since 1850, *Geophys. Res. Lett.*, *35*, L01706, doi:10.1029/2007GL032529.

Thompson, D. W. J., and J. M. Wallace (2000), Annular modes in the extratropical circulation. Part I: Month-to-month variability, *J. Clim.*, *13*, 1000–1016, doi:10.1175/1520-0442(2000)013<1000:AMITEC>2.0.CO;2.

Trenberth, K. E. (1997), The definition of El Niño, *Bull. Am. Meteorol. Soc.*, *78*, 2771–2777, doi:10.1175/1520-0477(1997)078<2771:TDOENO>2.0.CO;2.

Trenberth, K. E., and T. J. Hoar (1996), The 1990–1995 El Niño Southern Oscillation event: Longest on record, *Geophys. Res. Lett.*, *23*, 57–60, doi:10.1029/95GL03602.

Turner, J. (2004), Review: The El Niño–Southern Oscillation and Antarctica, *Int. J. Climatol.*, *24*, 1–31, doi:10.1002/joc.965.

Turner, J., and M. Row (1989), Mesoscale vortices in the British Antarctic Territory, in *Polar and Arctic Lows*, edited by P. F. Twitchell, E. A. Rasmussen, and K. L. Davidson, pp. 347–356, A. Deepak, Hampton, Va.

Turner, J., and J. P. Thomas (1994), Summer-season mesoscale cyclones in the Bellingshausen-Weddell region of the Antarctic and links with the synoptic-scale environment, *Int. J. Climatol.*, *14*, 871–894, doi:10.1002/joc.3370140805.

Turner, J., T. A. Lachlan-Cope, and J. P. Thomas (1993a), A comparison of Arctic and Antarctic mesoscale vortices, *J. Geophys. Res.*, *98*, 13,019–13,034, doi:10.1029/92JD02426.

Turner, J., T. A. Lachlan-Cope, D. E. Warren, and C. N. Duncan (1993b), A mesoscale vortex over Halley Station, Antarctica, *Mon. Weather Rev.*, *121*, 1317–1336, doi:10.1175/1520-0493(1993)121<1317:AMVOHS>2.0.CO;2.

van den Broeke, M. R. (1998), The semi-annual oscillation and Antarctic climate, Part 1, Recent changes, *Antarct. Sci.*, *10*, 184–191.

van Loon, H. (1966), On the annual temperature range over the southern oceans, *Geogr. Rev.*, *56*, 497–515, doi:10.2307/213055.

van Loon, H. (1967), The half-yearly oscillations in middle and high southern latitudes and the coreless winter, *J. Atmos. Sci.*, *24*, 472–486, doi:10.1175/1520-0469(1967)024<0472:THYOIM>2.0.CO;2.

van Loon, H. (1984), The Southern Oscillation, Part III: Associations with the trades and with the trough in the westerlies of the South Pacific Ocean, *Mon. Weather Rev.*, *112*, 947–954, doi:10.1175/1520-0493(1984)112<0947:TSOPIA>2.0.CO;2.

van Loon, H., and D. J. Shea (1985), The Southern Oscillation. Part 6: Anomalies of sea level pressure on the Southern Hemisphere and of Pacific sea surface temperature during the development of a warm event, *Mon. Weather Rev.*, *115*, 370–379.

van Loon, H., and J. W. Kidson (1993), The association between latitudinal temperature gradient and eddy transport, part 3, The Southern Hemisphere, *Aust. Meteorol. Mag.*, *42*, 31–37.

van Loon, H., and J. C. Rogers (1984), Interannual variations in the half-yearly cycle of pressure gradients and zonal wind at sea level on the Southern Hemisphere, *Tellus, Ser. A*, *36*, 76–86.

van Loon, H., and D. J. Shea (1985), The Southern Oscillation, part 4, The precursors south of 15°S to the extremes of the Oscillation, *Mon. Weather Rev.*, *113*, 2063–2074, doi:10.1175/1520-0493(1985)113<2063:TSOPIT>2.0.CO;2.

Wilhelmsen, K. (1985), Climatological study of gale-producing polar lows near Norway, *Tellus, Ser. A*, *37*, 451–459.

Yuan, X., and D. G. Martinson (2001), The Antarctic Dipole and its predictability, *Geophys. Res. Lett.*, *28*, 3609–3612, doi:10.1029/2001GL012969.

Yuan, X., D. G. Martinson, and W. T. Liu (1999), Effect of air-sea-ice interaction on winter 1996 Southern Ocean subpolar storm distribution, *J. Geophys. Res.*, *104*, 1991–2007, doi:10.1029/98JD02719.

Zahn, M., and H. von Storch (2008), A long-term climatology of North Atlantic polar lows, *Geophys. Res. Lett.*, *35*, L22702, doi:10.1029/2008GL035769.

A. M. Carleton, Department of Geography, Penn State University, University Park, PA 16802, USA.

C. Claud and B. Duchiron, Laboratoire de Météorologie Dynamique, IPSL, École Polytechnique, CNRS, Palaiseau F-91128, France. (chantal.claud@lmd.polytechnique.fr)

P. Terray, LOCEAN, IPSL, IRD, MNHN, Université Pierre et Marie Curie, CNRS, BP 100, 4 Place Jussieu, F-75005 Paris CEDEX, France.